Journal of Cleaner Production 313 (2021) 127753

Contents lists available at ScienceDirect

Journal of Cleaner Production

journal homepage: www.elsevier.com/locate/jclepro

Simulation of nitrogen dynamics in lowland polders using a new coupled modelling approach: Insights into management

Renhua Yan [a], Philip Brunner [b], Junfeng Gao [a,*]

[a] Key Laboratory of Watershed Geographic Sciences, Nanjing Institute of Geography and Limnology, Chinese Academy of Sciences, Nanjing, 210008, China
[b] Centre d'Hydrogéologie et de Géothermie, University of Neuchatel, Neuchatel, 2000, Switzerland

ARTICLE INFO

Handling editor: Bin-Chen

Keywords:
Lowland polders
Nitrogen modelling
Coupling
Paddy fields
Sensitivity analysis

ABSTRACT

A new modelling framework, the Polder Hydrology and Nitrogen modelling System (PHNS), was developed to simulate the nitrogen dynamics and processes in polder systems. PHNS is a mass-balance model that simulates water and nitrogen dynamics in soil and surface water systems through integrating the WALRUS-paddy, MUSLE, and INCA models. The model explicitly considers the interactions among surface water, groundwater, and vadose water, as well as irrigation, pumping, and fertilizer application, which are the key processes controlling the nitrogen cycle in polders. The sensitivity analysis, calibration, and validation of the developed model were conducted in a Chinese agricultural polder by using three years of measured hydro-meteorological data. The calibrated and validated results proved that the model has a good performance with an R^2 of 0.748 and a Nash-Sutcliffe (NS) efficiency coefficient of 0.619 for total nitrogen (TN) concentration during the validation period. The nitrogen budget results (net export of 40.4 kg/ha/yr) revealed that the polder is a nitrogen source for downstream freshwater systems. Reducing the amount of fertilizers, retaining crop residues, and restoring aquatic plants in surface water are effective countermeasures for reducing nitrogen export from polders. This study provides an efficient modelling tool and useful insights into polder management.

1. Introduction

To prevent floods and to reclaim new land, numerous polders have been built in the deltas, lakeside, and riverside areas in China and the Netherlands Brauer et al. (2014), (Su and Luo, 2019; Wang et al., 2019; Yan et al., 2017). A polder is a low-lying area that is separated from a river, lake, or sea by a dike (Fig. 1). A polder represents an isolated, artificial hydrologic unit, which mainly exchanges water with its surrounding through pumping and culvert infrastructure. To date, the polder areas in China have reached 4.07×10^5 km^2 (Wang et al., 2007), the majority of which lies in the middle and lower reaches of the Yangtze River (Lai et al., 2018; Yan et al., 2015) with a population of 0.2 billion protected. Moreover, the combination of flat topography, shallow groundwater, low hydraulic gradients, and dense water network results in numerous interactions between the surface water, groundwater, and vadose zone water in the polders.

Polders are used for intensive agriculture, and thus, they largely affect the water quality of downstream freshwater systems due to their wide distributions and more intense exploitation of agricultural land. High nitrogen concentrations have decreased the water quality of most Chinese lakes (Feng et al., 2012; Yu et al., 2019). Thus, an accurate estimation of the nitrogen loads exported from polders is critical for the sustainable management of aquatic systems downstream of or adjacent to polders. Because polders are associated with intense agricultural activities, polders are commonly viewed as nitrogen sources (Wang et al., 2011). However, several studies concluded that polders retain nitrogen pollution and outflow the water of low nitrates and suspended sediment concentration (Dausse et al., 2005; Ham et al., 2010). To quantify nitrogen dynamics in polders, identify if they constitute sinks or sources, and explore alternative management strategies, a suitable model that considers the relevant hydrological and transport processes in polders is urgently required.

Many models, e.g., the Soil and Water Assessment Tool (SWAT) (Neitsch et al., 2011), Agricultural Nonpoint Source (AGNPS) (Young et al., 1989), and the Xin'anjiang model (Zhao, 1992) have been designed to characterize hydrological and nutrient process at the catchment scale. However, when applied to a low-lying catchment with flat topography and enclosed dikes (i.e., polder), these models cannot realistically simulate the rainfall-runoff and nutrient processes. These models determine the flow routing based on elevation gradients using a

* Corresponding author. Nanjing Institute of Geography & Limnology, Chinese Academy of Sciences, 73 East Beijing Road, Nanjing, 210008, China.
E-mail address: gaojunf@niglas.ac.cn (J. Gao).

https://doi.org/10.1016/j.jclepro.2021.127753
Received 16 December 2020; Received in revised form 28 May 2021; Accepted 29 May 2021
Available online 3 June 2021

digital elevation model (DEM). As there are essentially no elevation gradients in polders, the flow routing is driven by the water level gradient. Besides, the groundwater-vadose zone coupling and the interaction between the surface water and groundwater feedback are not explicitly described in these models (Yan et al., 2018). Enclosed dikes, dense artificial drainage networks, and pumps control the polder inflow and outflow processes. Such situations are not explicitly considered in previous models. Recently, several modifications have been made to these models, including adding a virtual reservoir to control drainage (Li et al., 2013; Wang, 2006; Zhao et al., 2010), refining the DEM using real river networks and dikes to improve the watershed delineation (Luo et al., 2011), and introducing a drainage and irrigation module to manage the water in paddy fields (Lai et al., 2018). But they still do not accurately capture the characteristics of polder rainfall-runoff processes (Su and Luo, 2019) and related nitrogen dynamics in polders (Huang et al., 2018).

To address the above-identified knowledge and methodological gaps, this paper aims to (1) propose a polder hydrology and nitrogen modelling system by jointly simulating all relevant processes; (2) assess the model performance and its parameter sensitivity using the hydrological observations of Jianwei polder; (3) develop new water management strategies and discuss the function of a polder in nitrogen cycle based on the modelling case study. This study improves our understanding of polder processes and provides a scientific basis for developing effective measures to reduce the environmental risks associated with polders.

2. Methodology

2.1. Study area and data collection

2.1.1. Study area

The Jianwei polder has an area of 0.106 km^2 and is situated in the northwestern part of the Taihu Basin, Southeast China (Fig. 2). It is a representative Chinese agricultural polder in terms of its formation, hydrological situation, and agricultural use. As the polder is separated from the surrounding rivers by a dike, its water exchange with extra-territorial water is controlled by pumps and a culvert. Three pumping stations (P1 is used for draining floodwater; P2 and P3 are used for irrigation) and a culvert exist in the dike. The polder is dominated by farmland, including the paddy fields (50.1%) and drylands (21.7%) in the catchment area. The paddy fields are planted with a rice-wheat rotation system, wherein rice is grown from June to October and wheat is grown from November to May. The surface water including ditches and ponds takes up 9% of the total area. The reaming land (19.2%) is a residential area with around 100 permanent residents. Abundant inorganic fertilizers (compound fertilizer: N = 16%, P = 16%, K = 8%; urea: 46.4%) are applied by farmers to promote grain yield.

The Jianwei polder has a semi-tropical monsoon climate, with an annual average precipitation of 1082 mm, an annual mean temperature of 17 °C, and annual pan evaporation of 849 mm.

2.1.2. Data collection

The dataset required for the model consists of meteorological, land use, soil texture, vegetation coverage, discharge at the polder outlet, and water quality data. The detailed information about the measured data from our site was displayed in Table 1. The daily precipitation data were obtained from an on-site rain gauge and the daily temperature and pan evaporation data were from the nearest national weather station (Liyang station). The land use data were interpreted from Systeme Probatoire d'Observation de la Terre (SPOT) imagery. The soil texture data were determined based on soil samples collected from sites G1-3 (Fig. 2). The discharge at the polder outlet (Q) and the surface water level were used to calibrate the water quantity parameters. The discharge rates at the polder outlet (Q) included pumping and culvert discharges. The daily pumping discharge was calculated by multiplying the pumping capacity by the recorded running time. An automatic water level gauge was placed in the pond (SL1) to collect hourly surface water level data. The vegetation coverage index of the aquatic plants was measured monthly from sites V1–5.

The water quality data including particulate and dissolved nitrogen (PN and DN) and total nitrogen (TN) concentrations were obtained from water samples at sites W1–10. Water samples from site W1 (in the pond) were collected biweekly and were assumed to represent the surface water quality, and thus, they were used as observations for the calibration of the water quality parameters. The water samples at sites W2-3 were also collected biweekly to provide the irrigation water quality data during the irrigation period. Samples at W4–10 were collected from a rainfall-runoff event on August 24, 2013 to obtain the rainfall-runoff nutrient concentrations of the corresponding land use types. Sediment samples were collected from sites S1–3 once in 2013. The study period spanned from January 2014 to December 2016.

2.2. Model development

The Polder Hydrology and Nitrogen modelling System (PHNS) aims to reproduce the rainfall-runoff and nitrogen dynamics of lowland polders with strong artificial interventions and shallow groundwater. The framework provides the simulated results of daily nitrogen concentration, surface water level, discharge and nitrogen exports at the polder outlet and other intermediate variables (e.g., evapotranspiration, quickflow, and groundwater drainage of each land use type). The PHNS was developed by coupling three models, i.e., an improved version of Wageningen Lowland Runoff Simulator (WALRUS-paddy) (Yan et al., 2016), Modified Universal Soil Loss Equation (MUSLE) (Williams and Berndt, 1977), and Integrated Nitrogen in Catchments (INCA) models (Whitehead et al., 1998). The WALRUS-paddy model was developed as an extension of the WALRUS model (Brauer et al., 2014). It improves the

Fig. 1. Satellite image (left, from Google Earth) and aerial photograph (right, from Cui (2019)) of a lowland polder in the Taihu Basin, southeast China.

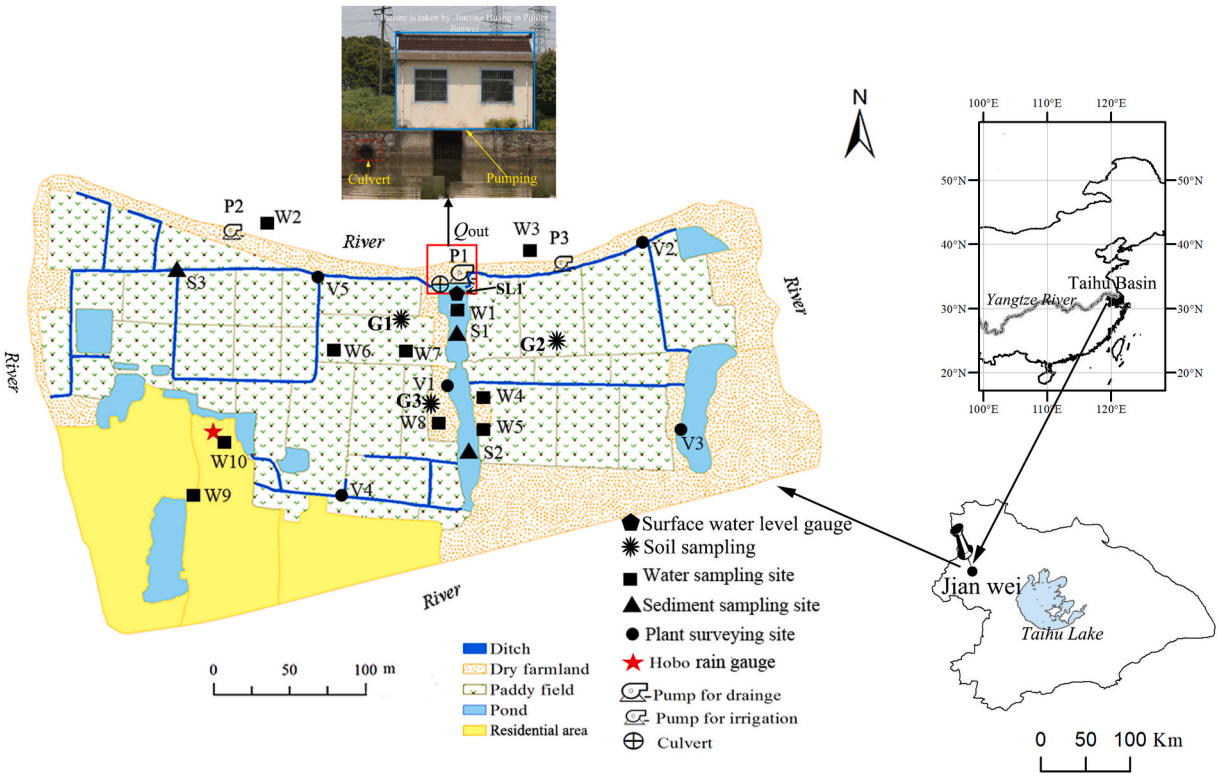

Fig. 2. The geographic location of the Jianwei polder and its sampling sites (modified from Yan et al. (2017)).

Table 1
Measured data from Jianwei polder.

Data type	Indicator	Source	Time series	Measuring frequency	Sampling points (Fig. 2)
Land use	Land use distribution and area	SPOT imagery interpretation and investigation	22 May 2014	_	
Soil	Particle size distribution and soil type	Soil sampling	2015	_	G1-3
Meteorology	Precipitation, temperature, and pan evaporation	Weather station	2014–2016	Daily	Liyang
Hydrology	Polder discharge, irrigation, amount, and surface water level	Recording and water level logger	2014–2016	Daily (discharge, irrigation) and hourly (surface water level)	P1-3, SL1
Water quality	Particulate nitrogen, dissolved nitrogen, and Total nitrogen	Water sampling	2014–2016	Biweekly (W1-3) and once (W4–10)	W1-10
	Total nitrogen	Sediment sampling	2014		S1-3
Management practice	Fertilization and crop planting	Farmer interviews	2014–2016	_	
Vegetation	Vegetation coverage index	Farmer interviews	2014–2016	Monthly	V1-5

polder rainfall-runoff processes by capturing the artificial inflow and outflow processes, the paddy irrigation, the groundwater-vadose zone coupling, and the interactions between the surface water and groundwater. The MUSLE model is one of the most widely used soil erosion models worldwide (Sadeghi et al., 2014; Williams and Berndt, 1977). The INCA model focuses on nitrate dynamics and considers plant uptake, surface and subsurface pathways, and multiple nitrogen sources such as atmospheric deposition, and the application of fertilizer. By combing these different models, the proposed PHNS model can simulate the processes from runoff generation to nutrient export in polder and it inherits the advantages of its respective component models. The PHNS emphasizes the feedbacks between the saturated and unsaturated zones, the groundwater–surface water interactions, the nitrogen-related physical and biological processes in the farmland and surface water, as well as the irrigation and drainage of the paddy fields.

The PHNS consists of water balance modules, paddy field and dryland nitrogen balance modules, and surface water nitrogen balance modules. The model's conceptual structure is shown in Fig. 3. Tables A1 and A2 present the model's equations, variables, and parameters.

2.2.1. *Water balance modules*

The WALRUS-paddy model was employed to simulate the water balance process in the polder. It comprises four modules: the dryland, paddy field, surface water, and residential area water balance modules. The dryland and paddy field modules include both a quickflow reservoir and a soil reservoir (a coupled vadose–groundwater reservoir). The

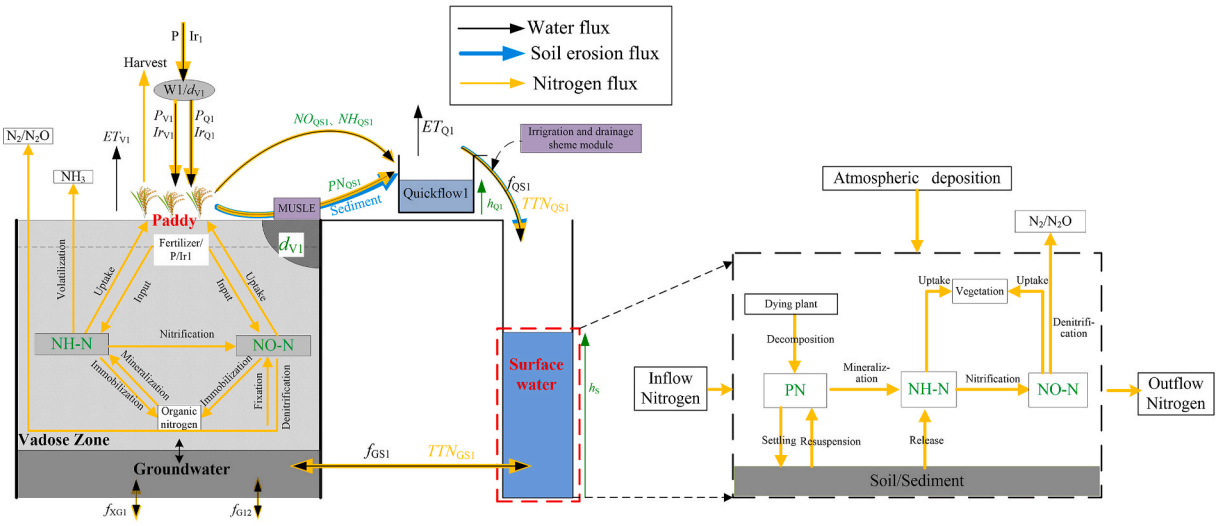

Fig. 3. Diagram showing the structure of the Polder Hydrology and Nitrogen modelling System (PHNS). The green variables are the state variables. The meaning of each variable is displayed in Tables A1 and A2.

storage deficit in the vadose zone (d_V, mm) determines both the evapotranspiration reduction (β) and the wetness index (W). W divides the precipitation into a portion that percolates to the soil matrix (P_V, mm/h) and another portion that flows by quickflow routes (P_Q, mm/h). The groundwater drainage or the infiltration of the surface water (f_{GS}, mm/h) is computed based on the differences in the water levels between the surface water (h_S, mm) and the groundwater (d_G, mm). The quickflow (f_{QS}, mm/h) consisting of overland flow, local ponding, and macropore flow, flows toward the surface water via a quickflow route rather than through the soil matrix. Additionally, the paddy field has an irrigation and drainage scheme with three critical water depths, which controls the complicated water management operations for optimal rice growth.

The irrigation water ($Ir1$, mm/h) is calculated as follows:

$$Ir1 = \begin{cases} h_{Q,\max 1} - h & if\ h_{Q1} < h_{Q,\min 1} \\ 0 & if\ h_{Q1} \geq h_{Q,\min 1} \end{cases} \quad (1)$$

where $h_{Q,\max 1}$ and $h_{Q,\min 1}$ represent the upper limit and the lower limit of the appropriate depth (mm), respectively.

The surface runoff in the paddy field (f_{QS1}, mm/h) is calculated as follows:

$$f_{QS1} = \begin{cases} \dfrac{h_{Q1} - H_{Q,\text{flood1}}}{c_{Q1}} \cdot a_{G1} & if\ h_{Q1} \geq h_{Q,\text{flood1}} \\ 0 & if\ h_{Q1} < h_{Q,\text{flood1}} \end{cases} \quad (2)$$

where h_{Q1} (mm) denotes the water level of the ponding water in the paddy fields. $h_{Q,\text{flood1}}$ denotes the maximum submergence-tolerant water level for rice growth, and c_{Q1} is the quickflow reservoir constant, which is determined during the calibration process.

For impervious residential areas, a runoff coefficient is used to estimate the runoff of residential areas. For the surface water, the water inflow components include precipitation (P_S, mm/h), paddy field drainage, dryland, and residential areas. Evapotranspiration (ET_S, mm/h) and catchment discharge (Q, mm/h) are the water outflow components. The culvert and pumping discharge constitute the total discharge at the polder outlet (Q, mm/h), which is computed by the relationships between the surface water level (h_S, mm) and the three threshold water levels (i.e., the threshold water levels to start culvert drainage ($h_{S_{\text{culvert}}}^{\text{start}}$, mm), to start pump drainage ($h_{S_{\text{pump}}}^{\text{start}}$, mm), and to stop pump drainage ($h_{S_{\text{pump}}}^{\text{stop}}$, mm)).

Q is estimated as follows

$$during\ the\ non-rice\ growth\ period:\ Q = \begin{cases} 0 & h_S < h_{S_{\text{culvert}}}^{\text{start}} \\ c_S \left(\dfrac{h_S - h_{S_{\text{culvert}}}^{\text{start}}}{c_D - h_{S_{\text{culvert}}}^{\text{start}}} \right)^{\gamma_S} & h_S > h_{S_{\text{culvert}}}^{\text{start}} \end{cases} \quad (3)$$

$$during\ the\ rice\ growth\ period:\ Q = \begin{cases} 0 & h_S < h_{S_{\text{pump}}}^{\text{start}} \\ Q_{\text{pumping}} & h_S > h_{S_{\text{pump}}}^{\text{start}} \text{ until } h_S = h_{S_{\text{pump}}}^{\text{stop}} \end{cases} \quad (4)$$

where Q_{pump} (mm/h) is obtained from converting the pump capacity (m^3/s) to mm/h by dividing by the polder area.

More details about the WALRUS-paddy model can be found in Yan et al. (2016). The equations for the various processes are presented in Table A1.

2.2.2. Paddy field and dryland nitrogen balance modules

The nitrogen is divided into two forms: particulate and dissolved nitrogen (PN and DN). The dissolved nitrogen is further parted into oxidized (nitrate/nitrite) nitrogen (NO), reduced (ammonium) nitrogen (NH). The INCA model is used to describe the NO and NH dynamics of the soil water in the farmland. The INCA model, which has been applied to catchments worldwide, is a process-based model that simulates the aquatic and land-related nitrogen cycles in a catchment. It was first proposed by Whitehead et al. (1998) and has been continually improved over the past decade (Wade et al. 2002a, 2002b). The INCA model simulates the NO processes related to fertilization, atmospheric deposition, irrigation, atmospheric nitrogen fixation, nitrification, denitrification, crop uptake, and runoff, and the NH processes related to fertilization, atmospheric deposition, irrigation, mineralization, nitrification, crop uptake, and runoff (Whitehead et al., 1998). Thus, the INCA model was utilized to track the NO and NH fluxes in the soil zone of the polder. Moreover, the MUSLE was selected to calculate the PN dynamics related to soil erosion.

1) The change in the NO and NH concentrations of the soil water in the paddy fields and drylands ($dNO_{\text{Soilwater},i}$ and $dNH_{\text{Soilwater},i}$) are computed as follows:

$$\frac{\mathrm{d}NO_{\mathrm{Soilwater},i}}{\mathrm{d}t}=\frac{TNO_{\mathrm{Atm}}+TNO_{\mathrm{fert},i}+TNO_{\mathrm{Ir},i}+TNO_{\mathrm{Fix},i}+TNH_{\mathrm{Nit},i}-TNO_{\mathrm{Denit},i}-TNO_{\mathrm{Upt},i}-f_{\mathrm{QS},i}/a_{\mathrm{G}i}\cdot NO_{\mathrm{Soilwater},i}^{t-dt}\Big/V_{\mathrm{Soilwater},i}\cdot 10^{-3}}{V_{\mathrm{Soilwater},i}}\cdot 10^{3} \tag{5}$$

$$\frac{\mathrm{d}NH_{\mathrm{Soilwater},i}}{\mathrm{d}t}=\frac{TNH_{\mathrm{Atm}}+TNH_{\mathrm{fert},i}+TNH_{\mathrm{Ir},i}+TPN_{\mathrm{Mi}.i}-TNH_{\mathrm{Vola},i}-TNH_{\mathrm{Nit},i}-TNH_{\mathrm{Immo},i}-TNH_{\mathrm{Upt},i}-f_{\mathrm{QS},i}/a_{\mathrm{G},i}\cdot NH_{\mathrm{Soilwater},i}^{t-dt}\Big/V_{\mathrm{Soilwater},i}\cdot 10^{-3}}{V_{\mathrm{Soilwater},i}}\cdot 10^{3} \tag{6}$$

where $TNO_{\mathrm{Atm}}/TNH_{\mathrm{Atm}}$, $TNO_{\mathrm{fert},i}/TNH_{\mathrm{fert},i}$, $TNO_{\mathrm{Ir},i}/TNH_{\mathrm{Ir},i}$, and $TNO_{\mathrm{Upt},i}/TNH_{\mathrm{Upt},i}$are the respective NO/NH mass changes attributed to atmospheric deposition, fertilization, irrigation, and uptake by plants, respectively (kg/m^2). $i \in [1, 2]$, where 1 represents the variable for the paddy fields, while 2 is the variable for the drylands. $TNO_{\mathrm{Fix},i}$ and $TPN_{\mathrm{Mi}.i}$are the NO and NH changes related to the NO fixation and the PN mineralization, respectively. $TNH_{\mathrm{Nit},i}$ and $TNO_{\mathrm{Denit},i}$are the NO changes due to nitrification and denitrification, respectively. $TNH_{\mathrm{Vola},i}$ and $TNH_{\mathrm{Immo},i}$ are the NH changes due to volatilization and immobilization, respectively. $NO_{\mathrm{Soilwater},i}{}^{t-dt}$ and $NH_{\mathrm{Soilwater},i}{}^{t-dt}$ are the NO and NH concentrations of the soil water at the beginning of the time step. Section 1 of the supplementary material provides details about the computational methods used for these variables, as well as an additional description of the INCA model.

The soil water (retention) volume, $V_{\mathrm{Soilwater},i}$ (m^3/m^2) is estimated with the storage deficit (d_{V}, m):

$$V_{\mathrm{Soilwater}} = T_{\mathrm{Soil}}\cdot p_{\mathrm{Soil}} - d_{\mathrm{V}} \tag{7}$$

where T_{Soil} is the thickness of the soil zone (m) and p_{Soil} is the soil porosity, the multiplication of which represents the maximum soil retention volume. d_{V} is obtained from the modelling results of the WALRUS-paddy model.

2) The PN concentration of the surface runoff associated with the soil erosion in the paddy fields and dryland areas is calculated as a function of soil erosion rate:

$$PN_{QS,i}=\frac{TPN_{\mathrm{sed},i}}{f_{\mathrm{QS},i}\cdot A}\cdot 10^{6} \tag{8}$$

$$TPN_{\mathrm{sed},i}=conc_{\mathrm{sedN},i}\cdot Sed_{,i}\cdot\lambda_{\mathrm{N:sed},i} \tag{9}$$

where $PN_{QS,i}$ is the PN concentration of the surface runoff from the farmland (mg/L). $i \in [1, 2]$, where the meanings are the same as above. $TPN_{\mathrm{sed},i}$ is the amount of PN loss attributed to soil erosion (kg/m^2). $f_{\mathrm{QS},i}$ is the quickflow (i.e., the surface runoff (mm/d), derived from simulated results of the WALRUS-paddy model), and A is the area of the catchment (m^2). $conc_{\mathrm{sedN},i}$ is the concentration of the nitrogen attached to the sediment in the farmland (measured), $\lambda_{\mathrm{N:sed},i}$ is the nitrogen enrichment ratio in the farmland, that is evaluated using the method described by Menzel (1980). $Sed_{,i}$is the amount of soil erosion, which is calculated using the MUSLE (Williams and Singh, 1995). The MUSLE is selected because it has been extensively incorporated in many environmental models (e.g., the SWAT and AGNPS models) (Sadeghi et al., 2014). More details about the MUSLE model can be found in Section 2 of the supplementary material.

2.2.3. Surface water nitrogen balance module

In this module, the source of the nitrogen in the surface water is runoff from each land use type and dry and wet atmospheric deposition; and it is exported through catchment discharge. So the changes in the PN, NO, and NH concentrations of the surface water (dNO_{S}, dNH_{S}, and dPN_{S}, respectively) are calculated as follows:

$$\frac{\mathrm{d}NO_{\mathrm{S}}}{\mathrm{d}t}=\frac{P_{\mathrm{S}}\cdot NO_{\mathrm{Pr}}+NO_{\mathrm{Drydeposition}}\cdot a_S\cdot 10^{6}+f_{\mathrm{QS}_1}\cdot NO_{\mathrm{QS1}}+f_{\mathrm{GS}1}\cdot NO_{\mathrm{GS1}}+f_{\mathrm{QS}_2}\cdot NO_{\mathrm{QS2}}+f_{\mathrm{GS2}}\cdot NO_{\mathrm{GS2}}+f_{\mathrm{rS}}\cdot NO_{\mathrm{rS}}}{h_{\mathrm{S}}\cdot a_{\mathrm{S}}+Q}+cNO_{\mathrm{S}} \tag{10}$$

$$\frac{\mathrm{d}NH_{\mathrm{S}}}{\mathrm{d}t}=\frac{P_{\mathrm{S}}\cdot NH_{\mathrm{Pr}}+NH_{\mathrm{Drydeposition}}\cdot a_S\cdot 10^{6}+f_{\mathrm{QS}_1}\cdot NH_{\mathrm{QS1}}+f_{\mathrm{GS}1}\cdot NH_{\mathrm{GS1}}+f_{\mathrm{QS}_2}\cdot NH_{\mathrm{QS2}}+f_{\mathrm{GS2}}\cdot NH_{\mathrm{GS2}}+f_{\mathrm{rS}}\cdot NH_{\mathrm{rS}}}{h_{\mathrm{S}}\cdot a_{\mathrm{S}}+Q}+cNH_{\mathrm{S}} \tag{11}$$

$$\frac{\mathrm{d}PN_{\mathrm{S}}}{\mathrm{d}t}=\frac{P_{\mathrm{S}}\cdot PN_{\mathrm{Pr}}+PN_{\mathrm{Drydeposition}}\cdot a_S\cdot 10^{6}+f_{\mathrm{QS}_1}\cdot PN_{\mathrm{QS1}}+f_{\mathrm{GS}1}\cdot PN_{\mathrm{GS1}}+f_{\mathrm{QS}_2}\cdot PN_{\mathrm{QS2}}+f_{\mathrm{GS2}}\cdot PN_{\mathrm{GS2}}+f_{\mathrm{rS}}\cdot PN_{\mathrm{rS}}}{h_{\mathrm{S}}\cdot a_{\mathrm{S}}+Q}+cPN_{\mathrm{S}} \tag{12}$$

where NO_{Pr}, NH_{Pr}, and PN_{Pr} denote the NO, NH, and PN concentrations of the precipitation (mg/L), respectively. NO_{QS1}, NH_{QS1}, and PN_{QS1} are the NO, NH, and PN concentrations of the quickflow from the paddy fields (mg/L), respectively. NO_{GS1}, NH_{GS1}, and PN_{GS1} denote the NO, NH, and PN concentrations of the groundwater drainage from the paddy fields (mg/L), respectively. NO_{QS2}, NH_{QS2}, and PN_{QS2} are the NO, NH, and PN concentrations of the quickflow from the dryland (mg/L), respectively, NO_{GS2}, NH_{GS2}, and PN_{GS2} denote the NO, NH, and PN concentrations of the groundwater drainage from the dryland (mg/L), respectively. NO_{rS}, NH_{rS}, and PN_{rS} are the NO, NH, and PN concentrations of the residential drainage (mg/L), respectively. h_S, Q, and a_S are the surface water level (mm), modelled catchment discharge (mm/h), and surface water area fraction, respectively. cNO_{S}, cNH_{S}, and cPN_{S} are the changes in the NO, NH, and PN concentrations of the surface water, respectively, which are caused by physical and biochemical processes (mg/L).

The physical and biochemical processes include nitrification, denitrification, mineralization, settling and resuspension, release from sediments, and uptake by plants, which are all taken into consideration by this module. As a result, cNO_{S}, cNH_{S}, and cPN_{S} are computed with the following functions:

$$cNO_{\mathrm{S}} = NH_{\mathrm{NitS}} - NO_{\mathrm{DenitS}} - NO_{\mathrm{UptS}} \tag{13}$$

$$cNH_{\mathrm{S}} = PN_{\mathrm{MiS}} + NH_{Re} - NH_{\mathrm{nitS}} - NH_{\mathrm{UptS}} \tag{14}$$

$$cPN_{\mathrm{S}} = PN_{Resuspension} - PN_{\mathrm{MiS}} - PN_{\mathrm{Settling}} \tag{15}$$

where NH_{NitS} (mg/L) is the change in the NH concentration due to

nitrification. NO_{DenitS} and NO_{UptS}(mg/L) are the changes in the NO concentration due to denitrification and plant uptake, respectively. PN_{MiS}(mg/L) is the change in the PN concentration due to mineralization. NH_{Re}, NH_{NitS}, and NH_{UptS} are the changes in the NH concentration due to mineralization, sediment release, nitrification, and plant uptake (mg/L), respectively. $PN_{Resuspension}$, PN_{MiS}, and $PN_{Settling}$ are the changes in the PN concentration due to resuspension, mineralization, and settling (mg/L), respectively. The computation methods for these variables can be seen in Table A2.

2.2.4. Model implementation

The WALRUS-paddy model code was written in R, while the original versions of the INCA and MUSLE models were programmed using other languages. For tight coupling, the INCA and MUSLE model codes were reprogrammed using R and then, they were integrated with the WALRUS-paddy model in the R language platform. PHNS runs at a daily time step. This model considers the heterogeneity of runoff and nitrogen among land use types. However, it assumes that soil texture, vegetation coverage, and other attributes are homogeneous within a specific land use type i.e., it does not account for spatial variation within a land use type.

The coupled model has 9 water quantity parameters and 28 water quality parameters to be calibrated (Tables A1 and A2). These parameters have physical meanings and represent specific catchment characteristics.

2.3. Model calibration and validation method

The water quantity parameters were calibrated with the observation data in 2015 and were validated with the data collected in 2016. Based on the optimized values of the water quantity parameters, the observation data for 2014–2015, and 2016 were used to calibrate and validate the water quality parameters, respectively. The initial conditions for d_G, h_S, NO_S, PN_S, h_Q, $NO_{QS,i}$, $NH_{QS,i}$, and $PN_{QS,i}$ have to be specified by the user, based on the observation made at the beginning of the period. The initial conditions for d_V were assumed to be the equilibrium value of the initial d_G ($d_{v,\ eq}$ (d_G)), which was automatically calculated based on d_G and the $d_{v,eq}$-d_G relationship (Table A1).

The calibration and validation processes related to the water quantity parameters have been carried out in Yan et al. (2019), which provided good modelled results for polder discharge and surface water level. In this study, only the calibration and validation of the water quality parameters were implemented, including sensitivity analysis, parameter calibration, and model validation.

2.3.1. Sensitivity analysis

The Latin Hypercube One-factor-At-a-Time (LH-OAT) method (Morris, 1991) was employed to identify the sensitive parameters in the nitrogen dynamics out of 28 water quality parameters (Table A2). This process reduced the amount of calibration work and facilitated the calibration of the most influential parameters in the subsequent step. The LH-OAT method combines the strengths of global and local sensitivity analysis, and it has been extensively used in sensitivity analysis cases (Hassanzadeh et al., 2018; Javaheri et al., 2018) and has been incorporated into the SWAT model. The Nash-Sutcliffe (NS) efficiency coefficient of the TN concentration of the surface water (TN_S) at site W1 (Fig. 2) was set as the objective function to determine the sensitivity.

The top 10 sensitive parameters, their meanings, and their relative sensitivities are listed in Table 2. The model was sensitive to $k_{PNmi,1}$, k_{NOupt}, $k_{NHupt,1}$, $k_{PNmi,2}$, $k_{NHupt,2}$, $k_{NHnit,\ 20}$$k_{NHupt}$$k_{NHnit,\ 20}$, k_{NHupt}, $k_{NHnit,1}$, $k_{NHre,\ 20}$, $k_{NOfix,1}$ in descending order. Although previous studies claimed that the parameter is sensitive when the relative sensitivity value larger than 0.2 and are generally sensitive when the relative sensitivity value larger than 0.05 (Huang and Zhang, 2010; Zhu et al., 2014), all the top 10 sensitive parameters (the relative sensitivity value ranged from 0.265 to 0.019) were chosen to be calibrated for making the model more likely to achieve the best performance.

Table 2
The top 10 sensitive parameters and their meanings, optimized values.

Parameter	Meaning	Range	Relative sensitivity value	Rank	Optimized value
$k_{PNmi,1}$	PN mineralization rate coefficient in the paddy soil store	0–0.46	0.265	1	2.973×10^{-10}
k_{NOupt}	NO uptake rate coefficient of plants in the surface water	0–2	0.148	2	1.964
$k_{NHupt,1}$	NH plant uptake rate coefficient in the paddy soil store	0.1–2	0.134	3	0.327
$k_{PNmi,2}$	PN mineralization rate coefficient in the dryland soil store	0–0.46	0.118	4	1.656×10^{-5}
$k_{NHupt,2}$	NH plant uptake rate coefficient in the dryland soil store	0.1–2	0.066	5	1.833
$k_{NHnit,\ 20}$	Nitrification rate coefficient in the surface water (20 °C)	0–1	0.047	6	0.845
k_{NHupt}	NH uptake rate coefficient of plants in the surface water	0–0.1	0.046	7	1.570×10^{-5}
$k_{NHnit,1}$	NH nitrification rate coefficient in the paddy soil store	0.02–0.11	0.041	8	0.102
$k_{NHRe,\ 20}$	Releasing rate coefficient of NH from sediment (20 °C)	0–0.11	0.025	9	0.102
$k_{NOfix,1}$	NO non-biological fixation rate coefficient in the soil store	0–0.036	0.019	10	8.390×10^{-6}

2.3.2. Parameter optimization

The 10 most sensitive parameters related to the nitrogen dynamics were automatically optimized by the Machine Coded Genetic Algorithm (MCGA). The Genetic Algorithm (GA) is a popular optimization tool for hydrological model calibration (Balov and Altunkaynak, 2019; Cheng et al., 2002, Reynolds Puga et al., 2018; Wang, 1991). Satman (2013) adopted a new encoding-decoding strategy for the GA and called it the MCGA. In this method, the classical crossover and mutation operations are based on byte representations of the variables instead of on the real-values. This improvement facilitates rapid calibration and tackles a broad search space with great accuracy. The calibration processes were carried out in the following way:

1) Definition of the objective function. The reciprocal of the NS of TN_S at W1 was selected as the objective function to assess the goodness of fit of each individual. The NS is one of the most popular and reliable statistic indices, aimed at evaluating the goodness of fit for hydrologic models (McCuen Richard et al., 2006).

$$F = \frac{1}{NS} = \frac{1}{1 - \frac{\sum_{i=1}^{n}\left(TNS_{obs,i} - TNS_{mod,i}\right)^2}{\sum_{i=1}^{n}\left(TNS_{obs,i} - \overline{TNS_{obs,i}}\right)^2}} \quad (16)$$

where $TNS_{mod,i}$ is the modelled nitrogen concentration at the time *i*; and $TNS_{obs,i}$ is the observed nitrogen concentration at time *i*. $\overline{TNS_{mod}}$ and $\overline{TNS_{obs}}$ represent the average values of the modelled and observed nitrogen concentrations, respectively. In this study, this was the minimization problem to obtain a higher NS. A population with a lower F value means higher goodness of fit.

2) Construction of an initial population (parameter sets). 200 populations were produced as the initial parameter sets of GA running. Here each parameter value was randomly generated between the lower bound and the upper bound of each parameter (Table 1). The number of parameters in each parameter set was the same as the number of parameters to be calibrated, i.e., 10.
3) Selection and reproduction. The population with a lower F (i.e., higher NS value) was selected and copied to the next generation. As a result, the general model fitness of the populations will be better and better over the iteration process.
4) Crossover and mutation. In each iteration, a crossover operator was applied to the byte representation of the populations to exchange parameter values. A mutation operator was also used in the byte representation to change the parameter values of the populations with a probability of 1%. Both operators formed new populations with better fitness.

5) Repetition of steps 2–4 until the iteration number reached the maximum value of 20. In the end, the population with the highest fitness was the best parameter set. From the first to the 12th generation, a significant improvement was achieved. After the 12th generation, the simulation error kept relatively stable. More information about MCGA calculation process can be seen in Satman (2013).

2.3.3. Model performance assessment

The NS and coefficient of determination (R^2) were applied to assess the model performance.

$$NS = 1 - \frac{\sum_{i=1}^{n}\left(N_{obs,i} - N_{mod,i}\right)^2}{\sum_{i=1}^{n}\left(N_{obs,i} - \overline{N_{obs,i}}\right)^2} \tag{17}$$

$$R^2 = \left(\frac{\sum_{i=1}^{n}\left(N_{mod,i} - \overline{N_{mod}}\right)\left(N_{obs,i} - \overline{N_{obs}}\right)}{\sqrt{\sum_{i=1}^{n}\left(N_{mod,i} - \overline{N_{mod}}\right)^2}\sqrt{\sum_{i=1}^{n}\left(N_{obs,i} - \overline{N_{obs}}\right)^2}}\right)^2 \tag{18}$$

where $N_{mod,i}$ is the simulated nitrogen concentration at the time *i*, and $N_{obs,i}$ is the measured nitrogen concentration at time *i*. $\overline{N_{mod}}$ and $\overline{N_{obs}}$represent the average values of the simulated and measured nitrogen concentrations, respectively.

3. Results

3.1. Calibration and validation results

A comparison of the modelled and observed nitrogen compositions of surface water (TN_S, DN_S, and PN_S) during the calibration and validation periods is shown in Fig. 4. The calibrated model has a good performance in *TN* modelling. The modelled TN_S values generally tracked the magnitudes and fluctuations of the observed values. The R^2 and NS values of TN_S were 0.526 and 0.505 during the calibration period and 0.748 and

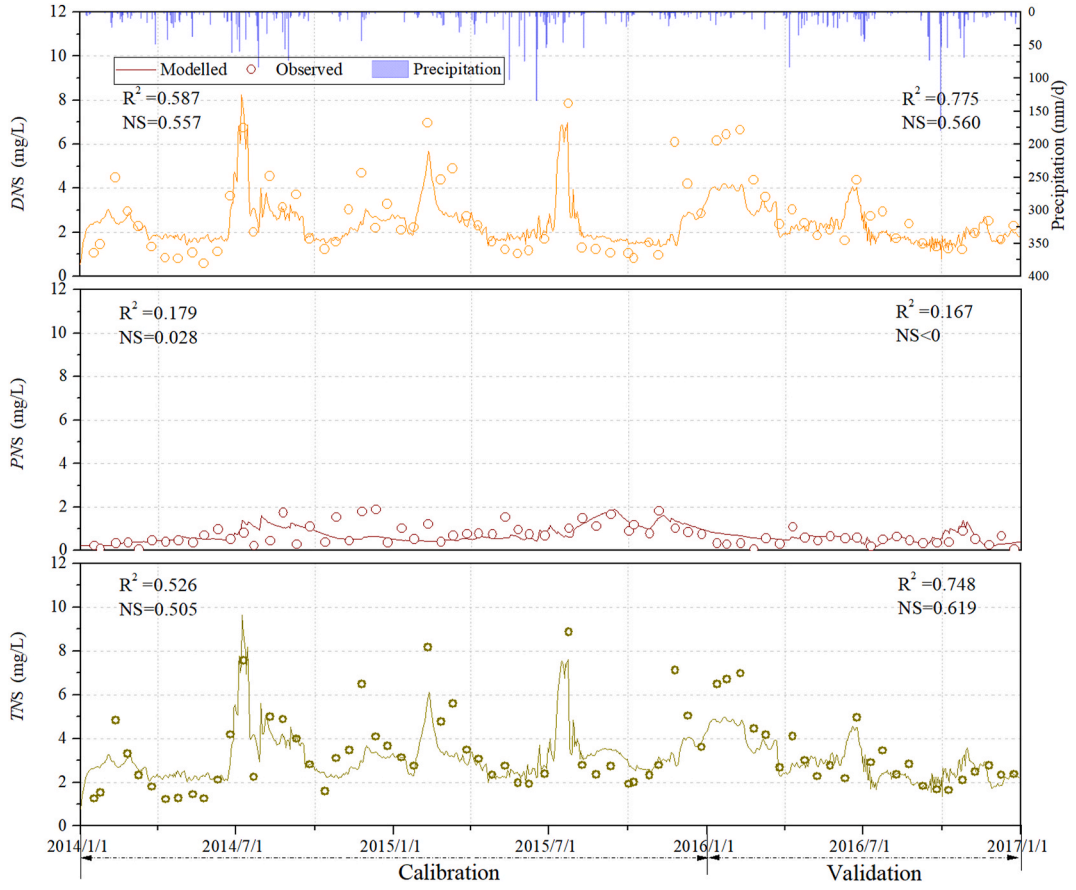

Fig. 4. Daily simulated and observed nitrogen of the surface water for the calibration period and the validation period. DN_S, PN_S, and TN_S are the dissolved nitrogen, particulate nitrogen, and total nitrogen of the surface water, respectively.

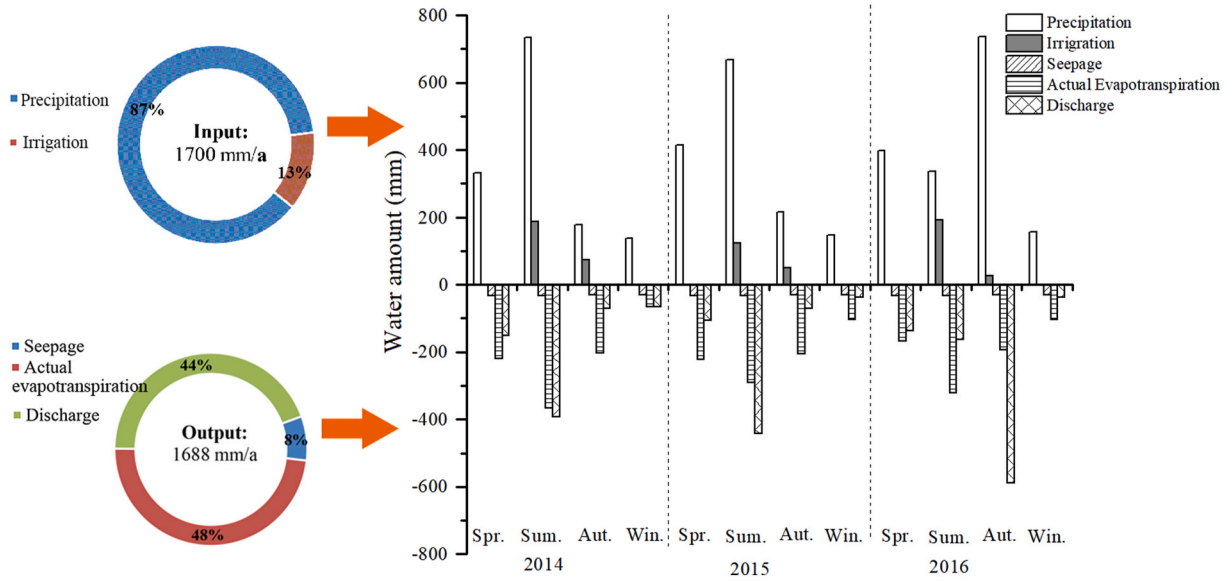

Fig. 5. Components of the annual water budget (left) and its seasonal changes (right). In the left panel, the input is the polder water entry, and the output denotes the polder water removal. In the right panel, the positive values denote the input components, while the negative values are the output components. All of the values are the corresponding flux divided by the polder area.

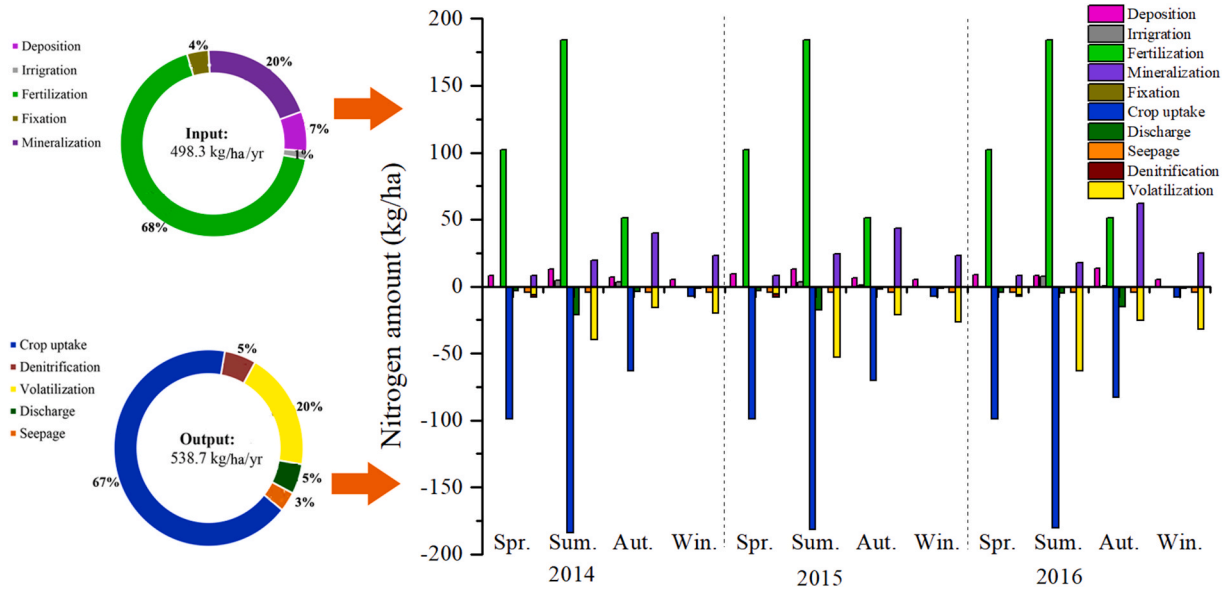

Fig. 6. Components of the annual nitrogen budget (left) and its seasonal changes (right). In the left panel, the input is the polder nitrogen entry, and the output denotes the polder nitrogen removal. In the right panel, the positive values denote the input components, while the negative values are the output components. All of the values are the corresponding flux divided by the polder area.

0.619 during the validation period, respectively. DN_S was reproduced slightly better than TN_S, with an R^2 of 0.587 and a NS of 0.557 during the calibration period, and an R^2 of 0.775 and an NS of 0.560 during the validation period. Furthermore, the cumulative modelled nitrogen form tracked well with that of the cumulative observed form (Fig. S1 in the supplementary material), which also indicated a good performance of the model. However, several deviations from the observations were found in the simulated DN_S and TN_S between January and March i.e., during the dry period.

3.2. Water budget

The average annual value of input water for the polder reached 1700 mm/yr (Fig. 5), 87% of which was precipitation and 13% of which was irrigation. Precipitation mostly occurred during summer and autumn due to the summer monsoon. Moreover, irrigation was executed in the summer and autumn to maintain a wet condition for optimal rice growth. The average annual amount of water output was 1688 mm/yr. Actual evapotranspiration and discharge were the two largest output items with percentages of 48% and 44%, respectively. The two items mostly occurred during summer and autumn because of the considerable precipitation and high temperature.

3.3. Nitrogen budget

The mean annual amount of TN input was 498.3 kg/ha/yr, while the TN output reached 538.7 kg/ha/yr (Fig. 6). Consequently, the net export of TN from the polder was 40.4 kg/ha/yr. TN input due to fertilization

(337.4 kg/ha/yr, converted from approximately 450 kg/ha/yr of farmland) was the largest, accounting for 68% of the total input. The mineralization of 101.2 kg/ha/yr contributed to the second largest nitrogen source with 20% of the total input. The atmospheric deposition of 34.1 kg/ha/yr contributed to 7% of the total input, including a wet deposition of 4% and a dry deposition of 3%. The fixation input of 18.7 kg/ha/yr and irrigation input of 6.9 kg/ha/yr were the smallest inputs, contributing 4% and 1% of the total TN input, respectively. The crop uptake of 360.6 kg/ha/yr contributed the most to the TN output (67%). After harvesting crops, most of the TN uptaken by crops was removed from agricultural land with the grains, and only 20–30% of TN was left in the form of straw and stubble (Duxbury et al., 2000), which decayed and returned TN to the soil system if conserved. NH volatilization had an estimate of 104.9 kg/ha/yr, contributing to 20% of TN output. The NO denitrification of 29.1 kg/ha/yr accounted for 5% of TN output. Discharge (26.6 kg/ha/yr) was a small TN output component, which had a larger value in summer and autumn compared to other seasons due to the uneven temporal distribution of the rainfall-runoff. Seepage (17.5 kg/ha/yr) constituted a small portion of the nitrogen output (3%).

The seasonal variations of the nitrogen budgets were found to be substantial, especially in terms of fertilization, crop uptake, and discharge. The amount of fertilizers applied by the local farmers in summer and spring were larger than those in other seasons. This is attributed to the fact that base fertilizer, seed fertilizer, and top dressing are mostly applied to farmland in summer and spring (Miao et al., 2011; Peng et al., 2010). The crop uptake was also larger in summer and spring than in other seasons. The nitrogen output through discharge increased in summer and autumn. The inter-annual changes in most of the nitrogen components were not significant.

4. Discussion

4.1. Model performance

Compared with the results of Wellen et al. (2015) reviewing 257 published modelling cases, the NS of our daily TN modelling (calibration period:0.505, validation period: 0.619) was close to or superior to the median value of the NS of the 257 cases (calibration period:0.540, validation period: 0.490), 66% of which used daily time steps and 35% of which used monthly time steps. Our model thus outperformed more than half of the previous cases. More importantly, our polder is more strongly affected by both strong human activities (e.g., frequent irrigation and drainage of paddy fields, multi-sourced runoff, and artificially controlled pump discharge) and the subtropical monsoon climate (e.g., uneven seasonal distributions of weather variables and frequent extreme precipitation events) than most of these previous cases (Yan et al., 2017). This situation substantially increases the challenges in the numerical simulation of the nitrogen processes in the polder (Brauer et al., 2014; Gaucherel et al., 2010; Yan et al., 2017). Even under these adverse conditions, our model still achieved favourable precision. Moreover, our simulated TN results are significantly better than those provided by the SWAT and AGNPS models for other polders of Southeast China (Sun, 2013; Xu, 2007; Zhu, 2010). Xu (2007) applied the SWAT model to simulate the TN of the Huoze polder and obtained a mean relative error of 20% for a short validation period of three and a half months, which is much higher than the mean relative error of 9% of our study for a three years' validation period. Sun (2013) simulated the Wangnan polder using the SWAT model and also had a higher mean relative error of 21% for a one-year's validation period. The application of the AGNPS model in Xueyan town showed a high relative error of 22% for one-day's validation period (Zhu, 2010). In addition, the estimated nitrogen balance components were compared with results from previous studies within the Taihu Basin to assess the reliability of our model results. The estimated mineralization of 101.2 kg/ha/yr, fixation of 18.7 kg/ha/yr, and atmospheric deposition of 34.1 kg/ha/yr were close to the corresponding values of 74–167.3 reported by Zhao et al. (2011), 13 kg/ha/yr by Hofmeier et al. (2015), and 28 kg/ha/yr by Hofmeier et al. (2015), respectively. The simulated ammonia volatilization of 104.9 kg/ha/yr, denitrification of 29.1 kg/ha/yr, and crop uptake of 360.6 kg/ha/yr were comparable to those of 71.5–147.9 kg/ha/yr by Zhao et al. (2012), 18.4–39.6 kg/ha/yr by Zhao et al. (2011), and 358 kg/ha/yr by Hofmeier et al. (2015), respectively. Specifically, the simulated crop uptake of 162.6 kg/ha/yr during rice season corresponded well with the one of 162.1 kg/ha/yr reported by Liang et al. (2021), and the estimated ammonia volatilization of 72.9 for rice season was also close to the one of 75 kg/ha/yr reported by Liang et al. (2021).

The general pattern of the changes in the DN_S was modelled slightly better than the TN_S concerning NS and R^2. In contrast, the PN_S modelling results had many inconsistencies with the observed PN_S and consequently had lower NS and R^2 values. Given that the model was mainly designed to simulate the *TN* dynamic and a small proportion of the *PN* (about 20%), this coupled model has a good performance for the nitrogen processes modelling. Since the rainfall-runoff processes mostly occur during the rainy period (from April to September) in the subtropical monsoon climatic zone, the polder outputs most of its annual amount of nitrogen during this period. Thus, the model can support non-point source management despite the discrepancies in the DN_S and TN_S in the dry period (between January and March). These discrepancies may be because the current model was designed to mainly express the nitrogen change driven by rainfall-runoff, while it does not finely characterize the change due to other factors (e.g., wind speed). For example, the winter monsoon wind can strongly stir the bottom mud (Shi et al., 2015), and thus it changes the nitrogen dynamic of the shallow surface water through sediment resuspension. This process was not considered in our model due to the complex relationship between the wind speed and the resuspension of sediment.

4.2. Sensitive parameters

The model was most sensitive to $k_{PNmi,1}$, k_{NOupt}, $k_{NHupt,1}$, $k_{PNmi,2}$, of which sensitivity values were higher than 0.1. $k_{PNmi,1}$ represents the PN mineralization rate coefficient in the paddy soil store, which determines the amount of organic nitrogen entering the inorganic nitrogen store. Mineralization was second only to fertilization as the largest nitrogen source and land use was dominated by paddy field; thus, the model was most sensitive to $k_{PNmi,1}$ with a sensitivity value of 0.265. $k_{PNmi,1}$ exerts about twice the influence of the second-ranked parameter. Due to a smaller area fraction of drylands than the paddy fields, the sensitivity value of $k_{PNmi,2}$ was smaller than that of $k_{PNmi,1}$ and ranked fourth. k_{NOupt} is the NO uptake rate coefficient of plants in surface water, that controls the removal rate of NO from the water via plant uptake. In particular, aquatic plants are manually reaped and removed from the water area in June to raise the water-passing capacity of ditches and ponds. This doing intercepts the releasing process of nitrogen into water effectively, which often occurs after aquatic plants wither and spoil. As a result, NO uptaken by plants is thoroughly removed via reaping. Such an irreversible uptake process led to a significant effect of k_{NOupt} on the simulated results and ranked $k_{NOupt}$to be second most sensitive. $k_{NHupt,1}$

indicates the NH plant uptake rate coefficient in the paddy soil store, which determines the process of taking an amount of NH away from the paddy soil store by the plant. The hot and humid climate and higher crop biomass increased the NH plant uptake rate and thus significantly affected the nitrogen balance of paddy soil. Therefore, $k_{NHupt,1}$ considerably influenced the nitrogen concentration of paddy rainfall-runoff and had a higher sensitivity value (0.134). Similar to the comparison results of $k_{PNmi,1}$ and $k_{PNmi,2}$, the sensitivity value of $k_{NHupt,2}$ was smaller than that of$k_{NHupt,1}$ and ranked fifth.

4.3. The role of a polder in the nitrogen cycle

The net export of 40.4 kg/ha/yr TN (i.e., an input of 498.3 kg/ha/yr minus output of 538.7 kg/ha/yr in Fig. 6) indicates that the lowland polder is an important TN source. Thus, it poses a threat to the downstream water quality and increases the risk of freshwater eutrophication. Moreover, the polder exported large quantities of nitrogen to the surrounding freshwater relative to the non-polder area in the Taihu Basin, which only exported 6.0–20.4 kg/ha/yr TN (Lai et al., 2006; Li et al., 2015, Taihu-Basin-Authority-of-Ministry-Of-Water-Resources, 2013). A high proportion of over-fertilization of croplands and the dense population in polder may explain its higher nitrogen export (Hofmeier et al., 2015; Lukianas et al., 2006; Yan et al., 2015).

Conversely, the total phosphorus (TP) budget in the same polder showed that the polder is a TP sink with net retention of 4.7 kg/ha/yr TP (Yan et al., 2017). The reason may be the differences in the compositions of the TN and TP nutrient forms. For TP, particulate phosphorus constitutes 72% of the TP and thus, TP is easily affected by the water regulation in the polder. Due to the hydraulic interception by the pumping station and dike, the retention of water in the pond substantially increases the duration of the settling process of particulate phosphorus, thereby decreasing the phosphorus export to the downstream rivers. In contrast, the dominant form of *TN* is *DN* (80%). DN is less likely to be affected by the hydraulic interception of the polder. Thus, the nitrogen concentration in the surface water remains high and is discharged into the surrounding water.

4.4. Implications of nitrogen budget and sensitivity analysis for management

4.4.1. Reducing fertilizer application and upgrading the energy consumption structure

The largest nitrogen input was farmland fertilization of 450 kg/ha/yr in the nitrogen budget analysis. This value falls within the range of the amount of TN application (from 423 to 756 N kg/ha/yr, reported by Zhou et al. (2012) for the rice-wheat rotation system in most of the Taihu Basin, but approaches the lower boundary value. The over-application of fertilizer is mostly adopted by local farmers to obtain high crop yields. This practice poses a major problem to sustainable agricultural development and water environment protection. The results of an experiment conducted in the Taihu Basin (Hofmeier et al., 2015) suggested a 27% reduction in nitrogen fertilization for the same cropping system, increasing the nitrogen use efficiency and reducing the nitrogen concentration of farmland runoff, while not decreasing crop yield. Thus, reducing fertilizer application by 27% is the most effective and economic measure for controlling the non-point pollution of lowland agricultural regions. Another major TN input was a deposition, 60% of which occurred in summer and autumn due to the much higher amount of precipitation during this period. The Taihu Basin, one of China's most developed areas, contains a large number of factories, high population density, and coal-based energy consumption (coal proportion: 52%–71%), which emits increasingly excessive amounts of anthropogenic nitrogen into the atmosphere (Lian et al., 2018). Consequently, this basin receives 34.1 kg/ha/yr of TN atmospheric deposition (wet deposition: 19.5 kg/ha/yr; and dry deposition: 14.6 kg/ha/yr), which is significantly larger than the mean global value of 9.31 kg/ha/yr (Jia, 2016). Upgrading the energy consumption structure and promoting cleaner industrial production would mitigate the atmospheric nitrogen deposition, thereby indirectly alleviating the agricultural non-point source pollution.

4.4.2. Retaining crop residues in croplands and increasing the coverage of aquatic plants in surface water

Crop uptake accounted for 67% of the TN output (360.6 TN kg/ha/yr). This uptake rate is comparable to the results of Hofmeier et al. (2015). After harvesting crops, most of the TN uptaken by crops is removed from agricultural lands with the grains, but the reaming straw and stubble are commonly burned by farmers. However, straw and stubble contain abundant nitrogen, especially summer rice residue accounting for nearly half of the TN uptaken by crops (Hofmeier et al., 2015; Miao et al., 2011). If these residues are not burned, the approximately 100 kg/ha/yr of organically bound nitrogen contained in the crop residues will be mineralized and will provide nitrogen for the next crop growing period (Hofmeier et al., 2015; Yang et al., 2008). Retaining crop residues is an agricultural practice recommended for reducing the export of nitrogen to surrounding water areas (Malhi et al., 2006).

The sensitivity analysis results showed that k_{NOupt} is the second most sensitive parameter (Section 2.3.1). This result implies that NO uptaken by plants in ditches and ponds considerably affects the nitrogen concentration of surface water, determining the amount of nitrogen output to downstream areas. Accordingly, implementing an aquatic vegetation restoration project to properly increase the coverage of plant species with high nitrogen uptake efficiency (such as cress, canna glauca, and *Hydrilla verticillata*) (Jin et al., 2017; Wang et al., 2010) and to apply ecological floating beds (Wang et al., 2018) is a supplementary pathway for reducing the nitrogen export to the surrounding river. Also, the increased aquatic vegetation coverage efficiently restrains the sediment resuspension induced by the wind and thus decreases the nitrogen concentration of the surface water (Shi et al., 2015).

4.5. Advantages, potential utilities, and disadvantages of the model

Our model is a coupled system composed of three different models, thereby inheriting the strengths of these models, specifically those of the WALRUS-paddy model. Compared with the existing models for simulating nitrogen dynamics in free drainage catchments, PHNS emphasizes the representation of several important processes of lowland polder. For instance, an irrigation and drainage scheme was used to generalize the complicated water management for paddy rice growth. Regulated discharge through pumping and a culvert at the polder outlet were computed using a function that involved surface water level (h_S) and three threshold water levels (i.e., the threshold water levels to start culvert drainage, to start pump drainage, and to stop pump drainage). A soil reservoir including the groundwater and unsaturated zones was introduced into the model to simulate the coupling of groundwater-unsaturated zones. Such operations increased the suitability of the model for modelling lowland polders and achieved precise results.

Moreover, the model has the advantages of a clear model structure, less forcing data (just conventional hydro-meteorological data), and shorter running time (one year of daily modelling takes less than 1 min).

The above-mentioned advantages promote the wide application of the model to water management and environmental risk assessment. For example, given that our model considers the rainfall-runoff, soil erosion, and nitrogen processes, this model and a methodology of quantifying the relationships between hydrological processes and environmental factors can be used to determine the key factors affecting the discharge, soil erosion, and nitrogen export from Chinese lowland polders. With the rapid population growth and increasing global changes, the effect of climate and land-use changes on the hydrological circle in lowland polders in the past, present, and future can be quantified by the proposed model. From the perspective of environmental engineering, the model can be used in the source apportionment of nitrogen from non-point sources, the estimation of water environmental capacity, and the reduction of pollution load. Addressing these issues is of significance for regional land use management and planning socio-economic activities. The combination of the model with a boosted regression tree algorithm analysis is applicable to investigating how hydrological variables respond to changes in environmental variables in different stages. Through this analysis, the pre-alarm values of a threshold level for steep changes in discharge, sediment, and nitrogen loss will be identified. These values provide critical parameters for catchment risk management and emergency planning, which can mitigate the flood and eutrophication crises to a large extent.

However, this model still has some limitations. Firstly, the model neglects nitrogen dynamics attributed to wind-driven sediment resuspension, limiting its ability to capture nitrogen change during the dry period. In fact, the effect of wind on sediment resuspension is markedly influenced by aquatic plant coverage, wind fetch, bed topography, bottom components, and water depth (Eleveld, 2012; Zhang et al., 2014). A resuspension model (Eleveld, 2012) combing with wind speed, linear fetch, and water depth can be incorporated into our model for defining critical conditions of sediment resuspension. Secondly, the surface water level was not observed in 2014. Consequently, the observed surface water level in 2015 and in 2016 were used to calibrate and validate the water quantity parameters, while the water quality parameters were calibrated and validated with the observation data for 2014–2015, and 2016. This temporal mismatch can potentially reduce the model's predictive capabilities. An additional field campaign will thus additionally increase the value of the model. Thirdly, the NS of TN was selected as the objective function to calibrate the parameters considering the model aiming at TN modelling. However, only including TN in the objective function might reduce the precision of components of TN, i.e., DN and PN. And the NS may overestimate the influence of peak values while it may underestimate the impact of low values (Krause et al., 2005, Legates and McCabe Jr 1999). Thus, collecting longer time series of data to optimize the water quantity and water quality parameters synchronously, including both the DN and PN in target function with appropriate weights, and employing other goodness-of-fit assessment indices (Such as R^2 and root mean square error (RMSE)) will be done in future work.

5. Conclusions

This study proposes a novel model (i.e., Polder Hydrology and Nitrogen modelling System (PHNS)) to address the problem of misrepresenting the polder characteristics encountered in previous conceptual models. The PHNS model considers the actual condition of Chinese polders, such as the multiple land-use types, tight surface water-groundwater-vadose water feedback, and highly regulated water practices. It was successfully tested in Jianwei polder, Southeast China using hydro-meteorological observation data, and acquired a good performance in terms of nitrogen modelling. The parameters related to the plant uptake, mineralization, and nitrification of nitrogen were identified as sensitive parameters. Accurate characterization of hydrological processes, less forcing data, and time-saving running facilitate the model application to academic research, water management, and environmental risk management.

The lowland polder is an important TN source, exporting more TN than other areas of the Taihu Basin. Abandoning over-fertilization, retaining straw and stubble, and increasing the coverage of aquatic plants in polder are recommended as measures to greatly alleviate this nutrient loss.

CRediT authorship contribution statement

Renhua Yan: Conceptualization, Methodology, Software, Formal analysis, Writing – original draft. **Philip Brunner:** Revise, Funding acquisition. **Junfeng Gao:** Supervision, Funding acquisition.

Declaration of competing interest

The authors declare that they have no known competing financial interests or personal relationships that could have appeared to influence the work reported in this paper.

Acknowledgements

The study was financed by the National Natural Science Foundation of China (42071052 and 41701031) and the Swiss Government Excellence Scholarship and State Scholarship Fund of China Scholarship Council (201804910378).

Appendix B. Supplementary data

Supplementary data to this article can be found online at https://doi.org/10.1016/j.jclepro.2021.127753.

Appendix A

Table A1
Main equations, variables, and parameters of the rainfall-runoff processes in the PHNS model (Yan et al., 2016). The subscript 1 represents the variable belonging to the paddy field, while the subscript 2 represents the variable belonging to the dryland.

	States	Paddy field (during the rice-growth period)	Dryland	Unit
d_V	Storage deficit	$\frac{dd\mathrm{V}1}{dt} = -\frac{f_{XG1} + P_{V1} + Ir_{V1} - ET_{V1} - f_{GS1} - f_{G12} + In1}{a_{G1}}$	$\frac{dd\mathrm{V}2}{dt} = -\frac{f_{XG2} + P_{V2} - ET_{V2} - f_{GS2} + f_{G12}}{a_{G2}}$	mm
D_G	Groundwater depth	$\frac{ddG1}{dt} = \frac{d\mathrm{V}1 - d\mathrm{V,eq}1}{c_{V1}}$	$\frac{ddG2}{dt} = \frac{d\mathrm{V}2 - d\mathrm{V,eq}2}{c_{V2}}$	mm
h_Q	Level quickflow reservoir	$\frac{dh\mathrm{Q}1}{dt} = \frac{P_{Q1} + Ir_{Q1} - ET_{Q1} - f_{QS1} - In_1}{a_{G1}}$	$\frac{dh\mathrm{Q}2}{dt} = \frac{P_{Q2} - f_{QS2}}{a_{G2}}$	mm
h_S	Surface water level	$\frac{dh_S}{dt} = -\frac{f_{XS} + P_S - ET_S + f_{GS} + f_{QS} + f_{rS} - Q}{a_S}$		mm
	Dependent variables			
W	Wetness index	$W1 = \mathrm{func}(d\mathrm{V}1)$	$W2 = \mathrm{func}(d\mathrm{V}2)$	
B	Evapotranspiration reduction factor	$\beta 1 = \mathrm{func}(d\mathrm{V}1)$	$\beta 2 = \mathrm{func}(d\mathrm{V}2)$	
$d_{V,eq}$	Equilibrium storage deficit	$d\mathrm{V,eq}1 = \mathrm{func}(d\mathrm{V}1)$	$d\mathrm{V,eq}2 = \mathrm{func}(d\mathrm{V}2)$	mm
	External fluxes: input			
P	Precipitation			mm/h
ET_{pot}	Potential evapotranspiration		$ET_{pot2} = E_0 \cdot C_K$	mm/h
E_0	Observed pan evaporation			mm/h
Q_{obs}	Observed discharge			mm/h
f_{XG}	Seepage (up/down)/extraction			mm/h
f_{XS}	Surface water supply/extraction			mm/h
	External fluxes: output			
ET_{act}	Actual evapotranspiration	$= ET\mathrm{V}1 + ET\mathrm{Q}1 + ET\mathrm{V}2 + ET\mathrm{S} + ET\mathrm{r}$		mm/h
Q	Modelled discharge	$= \mathrm{func}(h\mathrm{s})$		mm/h
$q_{peak,i}$	Peak runoff rate of paddy field and dryland	$= 3.79 \cdot (A \times 10^{-6})^{0.7} \cdot CS^{0.16} \cdot (f_{QS,i}/a_{Gi}/25.4)^{0.093 \cdot (A \times 10^{-6})^{0.017}} \cdot LW_i^{-0.19}$ Smith and Williams (1980)		m^3/s
	Internal fluxes			
P_S	Precipitation into surface water reservoir	$= P \cdot a_S$		mm/h
P_r	Precipitation into residual area	$= P \cdot a_r$		mm/h
Ir_1	Irrigation water into paddy field	$Ir1 = \begin{cases} h_{Q,max1} - h_{Q1} & h_{Q1} < h_{Q,min1} \\ 0 & h_{Q1} \geq h_{Q,min1} \end{cases}$		mm/h
P_V	Precipitation into vadose zone	$P_{V1} = \min(P, d\mathrm{V}1) \cdot a_{G1}$	$P_{V2} = P \cdot (1 - W2) \cdot a_{G2}$	mm/h
P_Q	Precipitation into quickflow reservoir	$P_{Q1} = P \cdot a_{G1} - P_{v1}$	$P_{Q2} = P \cdot W2 \cdot a_{G2}$	mm/h
Ir_{V1}	Irrigation water into a vadose zone of paddy field	$= \min(Ir1, d\mathrm{V}1) \cdot a_{G1}$		mm/h
Ir_{Q1}	Irrigation water into quickflow reservoir of paddy field	$= Ir1 \cdot a_{G1} - Irv1$		mm/h
In_1	Infiltration of the quickflow reservoir into the vadose zone in the paddy field	$In_1 = \min(d\mathrm{V}1, h_{Q1}) \cdot a_{G1}$ if $d\mathrm{V}1 > 0$ and $h_{Q1} > 0$; $In_1 = 0$ if $d\mathrm{V}1 = 0$ or $h_{Q1} = 0$		mm/h
ET_{act1}	Actual evapotranspiration of paddy field	$ET_{act1} = E_0 \cdot K_c$		mm/h
ET_{Q1}	Actual evapotranspiration from the quickflow reservoir of the paddy field	$ET_{Q1} \begin{cases} = \min(E_0, h_{Q1}) \cdot a_{G1} & \text{if } h_{Q1} > 0 \\ = 0 & \text{if } h_{Q1} = 0 \end{cases}$		mm/h
ET_V	Actual evapotranspiration vadose zone	$ET_{V1} = (ET\mathrm{act}1 - ET\mathrm{Q}1/a_{G1}) \cdot a_{G1}$	$ET_{V2} = ET\mathrm{pot}2 \cdot W2 \cdot a_{G2}$	mm/h
ET_r	Actual ET residential area	$= P \cdot (1 - \alpha) \cdot a_r$		mm/h
ET_S	Actual ET surface water	$= E_0 \cdot a_S$		mm/h

(continued on next page)

Table A1 (*continued*)

	States	Paddy field (during the rice-growth period)	Dryland	Unit
f_{GS}	Groundwater drainage/surface water infiltration	$f_{GS1} = \frac{(C_D - d_{G1} - h_S)\cdot\max(c_D - d_{G1}), hs)}{c_{G1}}.a_{G1}$	$f_{GS2} = \frac{(C_D - d_{G2} - h_S)\cdot\max(c_D - d_{G2}), hs)}{c_{G2}}.a_{G2}$	mm/h
f_{QS}	Quickflow	$f_{QS1} = \begin{cases} \frac{h_{Q1} - h_{Q,flood1}}{c_{Q1}}.a_{G1} & h_{Q1} \geq h_{Q,flood1} \\ 0 & h_{Q1} < h_{Q,flood1} \end{cases}$	$f_{QS2} = \frac{hQ2}{c_{Q2}}.a_{G2}$	mm/h
f_{rS}	Residential drainage	$= \alpha\cdot P\cdot a_r$		mm/h
f_{G12}	Groundwater flow between the paddy field and dryland	$= \frac{d_{G2} - d_{G1}}{c_{G3}}.a_{G1}$		mm/h
	Model parameters			
c_w	Wetness index parameter	c_{w1}	c_{w2}	mm
c_v	Vadose zone relaxation time	c_{v1}	c_{v2}	h
c_G	Groundwater reservoir constant	c_{G1}	c_{G2}	mm h
c_{G3}	Groundwater exchange constant between paddy field and dryland			mm h
c_Q	Quickflow reservoir constant	c_{Q1}	c_{Q2}	h
	Supplied parameters			
a_S	Surface water area fraction			
a_r	Residential area fraction			
a_G	Groundwater reservoir area fraction	a_{G1}	$a_{G2=}1- a_S - a_r - a_{G1}$	
A	Runoff coefficient of residential area			
K_c	Crop water requirement coefficient of paddy field			
C_K	Conversion coefficient from pan evaporation to potential evapotranspiration of dryland			
c_D	Channel depth			mm
	User-defined function with defaults			
$W(d_V)$	Wetness index	$W1 = \frac{1}{2} + \frac{1}{2}\cdot\cos\left(\frac{\max(\min(d_{V1}, c_{W1}), 0)\cdot\pi}{c_{W1}}\right)$	$W2 = \frac{1}{2} + \frac{1}{2}\cdot\cos\left(\frac{\max(\min(d_{V2}, c_{W2}), 0)\cdot\pi}{c_{W2}}\right)$	
$\beta(d_v)$	Evapotranspiration reduction factor	$\beta1 = \frac{ET_{act1}}{ET_{pot1}} = \frac{1}{2}\frac{1 - \exp[\zeta_1(d_{V1} - \zeta_2)]}{1 + \exp[\zeta_1(d_{V1} - \zeta_2)]} + \frac{1}{2}$	$\beta2 = \frac{ET_{act2}}{ET_{pot2}} = \frac{1}{2}\frac{1 - \exp[\zeta_1(d_{V2} - \zeta_2)]}{1 + \exp[\zeta_1(d_{V2} - \zeta_2)]} + \frac{1}{2}$	
$d_{v,eq}$ (d_G)	Equilibrium storage deficit	$dV, eq1 = \theta s1\left(dG1 - \frac{dG1^{1-1/b}}{(1-1/b)\phi_{ae1}^{-1/b}} - \frac{\phi_{ae1}}{1-b}\right)$	$dV, eq2 = \theta s2\left(dG2 - \frac{dG2^{1-1/b}}{(1-1/b)\phi_{ae2}^{-1/b}} - \frac{\phi_{ae2}}{1-b}\right)$	mm
$Q(h_S)$	Stage–discharge relation	non-rice growth period: $Q = \begin{cases} 0 & h_S \leq hS_{culvert}^{start} \\ c_S\left(\frac{h_S - hS_{culvert}^{start}}{c_D - hS_{culvert}^{start}}\right)^{\chi_s} & h_S > hS_{culvert}^{start} \end{cases}$	rice growth period: $Q = \begin{cases} 0 & h_S \leq h_{S_{pump}}^{start} \\ Q_{pumping} & h_S > h_{S_{pump}}^{start} \text{ until } h_S = h_{S_{pump}}^{stop} \end{cases}$	mm/h
	Parameters for default functions			
ζ_1	Curvature ET reduction function	ζ_{11}	ζ_{12}	
ζ_2	Translation ET reduction function	ζ_{21}	ζ_{22}	mm
B	Pore size distribution parameter	$b1$	$b2$	
Φ_{ae}	Air entry pressure	ϕ_{ae1}	ϕ_{ae2}	mm
θ_S	Soil moisture content at saturation	θ_{S1}	θ_{S2}	
c_S	Surface water parameter: bankfull Q			mm/h
x_s	Stage–discharge relation exponent			
$h_{S_{culvert}}^{start}$	Surface water level to start culvert drainage			mm
$h_{S_{pump}}^{start}$	Surface water level to start pump drainage			mm
$h_{S_{pump}}^{stop}$	Surface water level to stop pump drainage			mm
$h_{Q,min1}$	Lower limit of appropriate water level for the paddy field			mm
$h_{Q,max1}$	Upper limit of appropriate water level for the paddy field			mm
$h_{Q,flood1}$	Maximum submergence-tolerant water level for rice growth			mm

Table A2
Main equations, variables, and parameters of the nitrogen processes in the PHNS model. The subscript 1 represents the variable belonging to paddy field, while the subscript 2 represents the variable belonging to dryland.

NH_S	NH concentration of surface water	$\frac{dNH_S}{dt} = \frac{P_S \cdot NH_{Pr} + NH_{Drydeposition} \cdot a_S \cdot 10^6 + f_{QS1} \cdot NH_{QS1} + f_{GS1} \cdot NH_{GS1} + f_{QS2} \cdot NH_{QS2} + f_{GS2} \cdot NH_{GS2} + f_{rS} \cdot NH_{rS}}{h_S \cdot a_S + Q} + cNH_S$	0.522	mg/L
PN_S	PN concentration of surface water	$\frac{dPN_S}{dt} = \frac{P_S \cdot PN_{Pr} + PN_{Drydeposition} \cdot a_S \cdot 10^6 + f_{QS1} \cdot PN_{QS1} + f_{GS1} \cdot PN_{GS1} + f_{QS2} \cdot PN_{QS2} + f_{GS2} \cdot PN_{GS2} + f_{rS} \cdot PN_{rS}}{h_S \cdot a_S + Q} + cPN_S$	0.220	mg/L
$NO_{QS,i}$	NO concentration of quickflow in paddy field and dryland	$\frac{dNO_{Soilwater,i}}{dt} = \frac{TNO_{Atm} + TNO_{fert,i} + TNO_{Ir,i} + TNO_{Fix,i} + TNH_{Nit,i} - TNO_{Denit,i} - TNO_{Upt,i} - f_{QS,i}/a_{Gi} \cdot NO_{Soilwater,i}^{t-dt}/V_{Soilwater,i} \cdot 10^{-3}}{V_{Soilwater,i}} \cdot 10^3$		mg/L
$NH_{QS,i}$	NH concentration of quickflow in paddy field and dryland	$\frac{dNH_{Soilwater,i}}{dt} = \frac{TNH_{Atm} + TNH_{fert,i} + TNH_{Ir,i} + TPN_{Mi.i} - TNH_{Vola,i} - TNH_{Nit,i} - TNH_{Immo,i} - TNH_{Upt,i} - f_{QS,i}/a_{G,i} \cdot NH_{Soilwater,i}^{t-dt}/V_{Soilwater,i} \cdot 10^{-3}}{V_{Soilwater,i}} \cdot 10^3$		mg/L
$PN_{QS,i}$	PN concentration of quickflow associated with soil erosion in paddy field and dryland	$= \frac{TPN_{sed,i}}{f_{QS,i} \cdot A} \cdot 10^6$		mg/L
	1. Derived/calculated variables from water balance module			
h_S	Surface water level			mm
a_S	Surface water area fraction			
a_{Gi}	Paddy field and dryland area fraction			
P_S	Precipitation into surface water			mm/d
f_{XG}	Seepage (up/down)/extraction			mm/d
f_{QS1}	Quickflow of paddy field			mm/d
f_{QS2}	Quickflow of dryland			mm/d
f_{GS1}	Groundwater drainage of paddy field			mm/d
f_{GS2}	Groundwater drainage of dryland			mm/d
f_{rS}	Residential drainage			mm/d
Q	Modelled discharge			mm/d
$Ir_{,i}$	Irrigation water into paddy field and dryland			mm/d
	2. External variables: input			
	*3.*1 Paddy *field and dryland nitrogen balance modules*			
T_{Ave}	Daily average air temperature			°C
T_{Min}	Daily minimum air temperature			°C
T_{Max}	Daily maximum air temperature			°C
NO_{Pr}	NO concentration of precipitation		1.10	mg/L
NH_{Pr}	NH concentration of precipitation		0.08	mg/L
PN_{Pr}	PN concentration of precipitation		0.25	mg/L
$NO_{Drydeposition}$	NH of dry deposition		3.3×10^{-7}	kg/m^2
$NH_{Drydeposition}$	NO of dry deposition		1.1×10^{-6}	kg/m^2
$PN_{Drydeposition}$	PN of dry deposition		2.1×10^{-6}	kg/m^2
$TNO_{fert,i}$	NO input attributed to fertilization in paddy field and dryland		0–0.56	kg/m^2/d

(*continued on next page*)

Table A2 (*continued*)

NH_S	NH concentration of surface water	$\frac{dNH_S}{dt} = \frac{P_S \cdot NH_{Pr} + NH_{Drydeposition} \cdot a_S \cdot 10^6 + f_{QS1} \cdot NH_{QS1} + f_{GS1} \cdot NH_{GS1} + f_{QS2} \cdot NH_{QS2} + f_{GS2} \cdot NH_{GS2} + f_{rS} \cdot NH_{rS}}{h_S \cdot a_S + Q} + cNH_S$	0.522	mg/L
$TNH_{fert,i}$	NO input attributed to fertilization in paddy field and dryland		0–2.22	kg/m^2/d
$conc_{sedN,i}$	Concentration of nitrogen attached to sediment in paddy field and dryland			kg/kg soil
$\lambda_{N:sed,i}$	Enrichment ratio of nitrogen in paddy field and dryland			
	3.2 Surface water nitrogen balance module			
PN_{GS1}	PN concentration of groundwater drainage from paddy field drainage		0.33	mg/L
PN_{GS2}	PN concentration of groundwater drainage from dryland		1.12	mg/L
NO_{GS1}	NO concentration of groundwater drainage from paddy field		3.77	mg/L
NO_{GS2}	NO concentration of groundwater drainage from dryland		27.37	mg/L
NH_{GS1}	NH concentration of groundwater drainage from paddy field		0.79	mg/L
NH_{GS2}	NH concentration of groundwater drainage from dryland		5.76	mg/L
PN_{rS}	PN concentration of residential drainage		1.42	mg/L
NO_{rS}	NO concentration of residential drainage		1.08	mg/L
NH_{rS}	NH concentration of residential drainage		1.25	mg/L
PN_{river}	PN concentration of surrounding river		0.06–2.71	mg/L
NO_{river}	NO concentration of surrounding river		0.34–2.71	mg/L
NH_{river}	NH concentration of surrounding river		0.34–2.71	mg/L
TN_{sed}	TN concentration of sediment pore water		0.10	mg/L
DO_S	Dissolved oxygen concentration of surface water		4.30–11.2	mg/L
	3. External variables: output			
TTN_Q	Nitrogen export amount attributed to culvert and pumping discharge	$= Q \cdot (NO_S + NH_S + PN_S) \cdot A \cdot 10^{-6}$		kg
	4. Internal variables			
	*5.*1 Paddy *field and dryland nitrogen balance modules*			
$TNO_{Fix,\ i}$	NO input attributed to fixation in paddy field and dryland	$= k_{NOfix,i} \cdot 1.047^{T_{soil}-20}$		kg/m^2
$TNH_{Nit,i}$	NO input attributed to NH nitrification in paddy field and dryland	$= \frac{k_{NHnit,i} \cdot 1.047^{T_{soil,i}-20} \cdot f_{dv,i} \cdot NH_{Soilwater,i}^{\ t-dt}}{V_{Soilwater,i}}$		kg/m^2
$TNO_{Denit,i}$	NO export attributed to denitrification in paddy field and dryland	$= \frac{k_{NOdenit,i} \cdot 1.047^{T_{soil,i}-20} \cdot f_{dv,i} \cdot NO_{Soilwater,i}^{\ t-dt}}{V_{Soilwater,i}}$		kg/m^2
$TNO_{Upt,i}$	NO export attributed to plant uptake in paddy field and dryland	$= \frac{k_{NOupt,i} \cdot 1.047^{T_{soil,i}-20} \cdot f_{dv,i} \cdot f_{plantgrowth} \cdot NO_{Soilwater,i}^{\ t-dt}}{V_{Soilwater,i}}$		kg/m^2
$TPN_{PNmi,i}$	NH input attributed to PN mineralization	$= k_{PNmi,i} \cdot 1.047^{T_{soil,i}-20} f_{dv,i}$		kg/m^2

(*continued on next page*)

Table A2 (*continued*)

NH_S	NH concentration of surface water	$\frac{dNH_S}{dt} = \frac{P_S \cdot NH_{Pr} + NH_{Drydeposition} \cdot a_S \cdot 10^6 + f_{QS1} \cdot NH_{QS1} + f_{GS1} \cdot NH_{GS1} + f_{QS2} \cdot NH_{QS2} + f_{GS2} \cdot NH_{GS2} + f_{rS} \cdot NH_{rS}}{h_S \cdot a_S + Q} + cNH_S$	0.522	mg/L
$TNH_{Vola,i}$	NH export attributed to volatilization in paddy field and dryland	$= \frac{k_{NHvola,i} \cdot 1.047^{T_{soil,i}-20} \cdot 0.15 \cdot f_{dv1} \cdot NH_{Soilwater,i}{}^{t-dt}}{V_{Soilwater,i}}$		kg/m^2
$TNH_{Immo,i}$	NH export attributed to immobilization in paddy field and dryland	$= \frac{k_{NHimmo,i} \cdot 1.047^{T_{soil,i}-20} \cdot f_{dv1} \cdot NH_{Soilwater,i}{}^{t-dt}}{V_{Soilwater,i}}$		kg/m^2
$TNH_{Upt,\ i}$	NH export attributed to plant uptake in paddy field and dryland	$= \frac{k_{NHupt,i} \cdot 1.047^{T_{soil,i}-20} \cdot f_{dv,i} \cdot f_{plantgrowth} \cdot NH_{Soilwater,i}{}^{t-dt}}{V_{Soilwater,i}}$		kg/m^2
$TNO_{Ir,i}$	NO input attributed to irrigation in paddy field and dryland	$= \frac{Ir_{V,i}}{a_{G,i}} NO_{river} \cdot 10^{-6}$		kg/m^2
$TNH_{Ir,i}$	NH input attributed to irrigation in paddy field and dryland	$= \frac{Ir_{V,i}}{a_{G,i}} NH_{river} \cdot 10^{-6}$		kg/m^2
TNO_{Atm}	NO mass due to atmospheric deposition	$= P \cdot NO_{Pr} \cdot 10^{-6} + NO_{Drydeposition}$		kg/m^2
TNH_{Atm}	NH mass due to atmospheric deposition	$= P \cdot NH_{Pr} \cdot 10^{-6} + NH_{Drydeposition}$		kg/m^2
T_S	Surface water temperature	$= 0.9475 \cdot T_{Ave}$		°C
$T_{Soil,i}$	soil water temperature	$= T_{Ave} - (T_{Max} - T_{Min}) \sin\left(\frac{3\pi day_{i,year}}{2.365}\right)$		°C
$TPN_{sed,i}$	PN export attributed to soil erosion in paddy field and dryland	$= conc_{sedN,i} \cdot Sed_i \cdot \lambda_{N:sed,i}$		kg/d
Sed,i	Amount of soil erosion	$= 11.8 \cdot (0.001 \cdot f_{QS,i} \cdot q_{peak,i} \cdot A)^{0.56} \cdot K_i \cdot C_i \cdot P_{control,i} \cdot LS_i \cdot CFRG_i \cdot 100$		kg/d
	5.2 Surface water nitrogen balance module			
cNO_S	NO concentration change attributed to physical and biochemistry process in surface water	$= NH_{NitS} - NO_{DenitS} - NO_{UptS}$		mg/L
cNH_S	NH concentration change attributed to physical and biochemistry process in surface water	$= PN_{MiS} + NH_{Re} - NH_{nitS} - NH_{UptS}$		mg/L
cPN_S	PN concentration change attributed to physical and biochemistry process in surface water	$= PN_{Resuspension} - PN_{MiS} - PN_{Settling}$		mg/L
NH_{NitS}	NH concentration change due to nitrification in surface water	$= k_{NHnit,\ 20} \cdot (1 - \exp(-0.6 \cdot DO_S)) \cdot 1.083^{T_S-20} \cdot NH_S{}^{t-dt}$		mg/L
NO_{DenitS}	NO concentration change due to denitrification in surface water	$= k_{NOdenit,\ 20} \cdot \exp\left(-0.02(T_S-20)^2\right) \cdot \frac{K_{DOhdenit}}{K_{DOhdenit} + DO_S} \cdot \frac{NO_S{}^{t-dt}}{K_{NOhdenit} + NO_S{}^{t-dt}} \cdot NO_S{}^{t-dt}$		mg/L
NO_{UptS}	NO concentration change due to plant uptake in surface water	$= k_{NOupt} \cdot \frac{NO_S{}^{t-dt}}{K_{NOhupt} + NO_S{}^{t-dt}} \cdot \frac{T_{Ave} - T_{Min}}{T_{Max} - T_{Min}} \cdot NO_S{}^{t-dt}$		mg/L
PN_{MiS}	PN concentration change due to mineralization	$= k_{PNmi,\ 20} \cdot 1.047^{T_S-20} \cdot PN_S{}^{t-dt}$		mg/L
NH_{Re}	NH concentration change due to sediment releasing	$= k_{Re,\ 20} \cdot 1.047^{T_S-20} \cdot TN_{sed}$		mg/L
NH_{UptS}	NH concentration change due to plant uptake in surface water	$= k_{NHupt} \cdot \frac{NH_S{}^{t-dt}}{K_{NHhupt} + NH_S{}^{t-dt}} \cdot \frac{T_{Ave} - T_{Min}}{T_{MaxMin}} \cdot NH_S{}^{t-dt}$		mg/L
$PN_{Resuspension}$	PN concentration change due to resuspension in surface water	$= k_{PNresuspension} \cdot \frac{T_{Ave} - T_{Min}}{T_{Max} - T_{Min}}$		mg/L
$PN_{Settling}$	PN concentration change due to settling in surface water	$= k_{PNsettling,\ 20} \cdot 1.024^{T_S-20} \cdot PN_S{}^{t-dt}$		mg/L
	5. Model parameters			
	*6.*1 Paddy *field and dryland nitrogen balance modules*			

(*continued on next page*)

Table A2 (*continued*)

NH_S	NH concentration of surface water	$\frac{dNH_S}{dt} = \frac{P_S \cdot NH_{Pr} + NH_{Drydeposition} \cdot a_S \cdot 10^6 + f_{QS1} \cdot NH_{QS1} + f_{GS1} \cdot NH_{GS1} + f_{QS2} \cdot NH_{QS2} + f_{GS2} \cdot NH_{GS2} + f_{rS} \cdot NH_{rS}}{h_S \cdot a_S + Q} + cNH_S$	0.522	mg/L
$k_{NOfix,i}$	NO Non-biological fixation rate coefficient in the soil store		0–0.036	kg/m^2
$k_{NHnit,i}$	NH nitrification rate coefficient in the soil store		0.02–0.1	m/d
$k_{NOdenit,i}$	NO denitrification rate coefficient in the soil store		0.02–0.8	m/d
$k_{NOupt,i}$	NO plant uptake rate coefficient in the soil store		0.1–2	m/d
$k_{PNmi,i}$	PN mineralization rate coefficient in the soil store		0–0.46	kg/m^2
$k_{NHvola,i}$	NH volatilization rate coefficient in the soil store		0.03–0.8	m/d
$k_{NHimmo,i}$	NH immobilization rate coefficient in the soil store		0–0.05	m/d
$k_{NHupt,i}$	NH plant uptake rate coefficient in the soil store		0.1–2	d^{-1}
$f_{dv,i}$	Storage deficit factor	$= \frac{d_{Vmax,i} - d_{V1,i}}{d_{Vmax,i}}$		
$f_{plantgrowth}$	Seasonal plant growth factor representing the change in crop demand for nitrogen	$= 0.66 + 0.34 \cdot \sin\left(2\pi \frac{day_{j,year} - day_{j,start}}{365}\right)$		
	6.2 Surface water nitrogen balance module			
$k_{NHnit,\ 20}$	Nitrification rate coefficient in the surface water (20 °C)		0–0.4	d^{-1}
$k_{NOdenit,\ 20}$	Denitrification rate coefficient in the surface water (20 °C)		0–0.05	d^{-1}
k_{NOupt}	NO uptake rate coefficient of plants in the surface water		0–0.3	d^{-1}
$k_{PNmi,\ 20}$	Mineralization rate coefficient in the surface water (20 °C)		0–0.02	d^{-1}
$k_{NHRe,\ 20}$	Releasing rate coefficient of NH from sediment (20 °C)		0–0.1	d^{-1}
k_{NHupt}	NH uptake rate coefficient of plants in the surface water		0–0.1	d^{-1}
$k_{PNresuspension}$	PN resuspension rate coefficient from sediment		0–0.01	mg/L
$k_{PNsettling,\ 20}$	PN settling rate coefficient to sediment (20 °C)		0–0.125	d^{-1}
$K_{DOhdenit}$	Half saturation constant of DO for denitrification		0.1–0.5	mg/L
$K_{NOhdenit}$	Half saturation constant of NO for denitrification		0.1–0.5	mg/L
K_{NOhupt}	Half saturation constant of NO for plant uptake		0.1–0.5	mg/L
K_{NHhupt}	Half saturation constant of NH for plant uptake		0.1–0.3	mg/L
	Supplied parameters			
A	Polder area		106,000	m^2
a_S	Surface water area fraction		0.09	
K_i	Soil erodibility factor of paddy field and dryland			
C_i	Vegetation cover and management factor of paddy field and dryland			
$P_{control,i}$	Soil erosion control practice factor of paddy field and dryland			
LS_i	Topographic factor of paddy field and dryland			
$CFRG_i$	Coarse fragment factor of paddy field and dryland			

Compliance with ethical standards

The authors declare that they have no conflict of interest. This article does not contain any studies with human participants or animals performed by any of the authors. Informed consent was obtained from all individual participants included in the study.

References

Balov, M.N., Altunkaynak, A., 2019. The impacts of climate change on the runoff volume of Melen and Munzur Rivers in Turkey based on calibration of WASMOD model with multiobjective genetic algorithm. Meteorol. Atmos. Phys. 1–14.

Brauer, C., Teuling, A., Torfs, P., Uijlenhoet, R., 2014. The Wageningen Lowland Runoff Simulator (WALRUS): a lumped rainfall–runoff model for catchments with shallow groundwater. Geosci. Model Dev. (GMD) 7 (5), 2313–2332.

Cheng, C.-T., Ou, C., Chau, K., 2002. Combining a fuzzy optimal model with a genetic algorithm to solve multi-objective rainfall–runoff model calibration. J. Hydrol 268 (1–4), 72–86.

Cui, Z., 2019. Modeling the response of river nutrient conditions to land use changes in lowland artificial watersheds (polders). Ecol. Eng. 135, 98–107.

Dausse, A., Mérot, P., Bouzillé, J.B., Bonis, A., Lefeuvre, J.C., 2005. Variability of nutrient and particulate matter fluxes between the sea and a polder after partial tidal restoration, Northwestern France. Estuarine. Coastal and Shelf Science 64 (2), 295–306.

Duxbury, J., Abrol, I., Gupta, R., Bronson, K., 2000. Long-term Soil Fertility Experiments with Rice–Wheat Rotations in South Asia. Rice Wheat Consortium for the Indo-Gangetic Plains. RWC/CIMMYT, New Delhi.

Eleveld, M.A., 2012. Wind-induced resuspension in a shallow lake from Medium Resolution Imaging Spectrometer (MERIS) full-resolution reflectances. Water Resour. Res. 48 (4).

Feng, W., Zhan, J., Deng, X., 2012. Influencing factors of lake eutrophication in China–A case study in 22 lakes in China. Ecology & Environmental Sciences 21 (1), 94–100.

Gaucherel, C., Martinet, V., Bamière, L., Sheeren, D., Gibon, A., Joannon, A., Castellazzi, M., Boussard, H., Barraquand, F., Inchausti, P., 2010. A Multidisciplinary Modelling Approach to Analyse and Predict the Effects of Landscape Dynamics on Biodiversity.

Ham, J., Yoon, C.G., Kim, H.-J., Kim, H.-C., 2010. Modeling the effects of constructed wetland on nonpoint source pollution control and reservoir water quality improvement. J. Environ. Sci. 22 (6), 834–839.

Hassanzadeh, Y., Afshar, A.A., Pourreza-Bilondi, M., Memarian, H., Besalatpour, A.A., 2018. Toward a combined Bayesian frameworks to quantify parameter uncertainty in a large mountainous catchment with high spatial variability. Environ. Monit. Assess. 191 (1), 23.

Hofmeier, M., Roelcke, M., Han, Y., Lan, T., Bergmann, H., Böhm, D., Cai, Z., Nieder, R., 2015. Nitrogen management in a rice–wheat system in the Taihu Region: recommendations based on field experiments and surveys. Agric. Ecosyst. Environ. 209, 60–73.

Huang, J., Arhonditsis, G.B., Gao, J., Kim, D.-K., Dong, F., 2018. Towards the development of a modeling framework to track nitrogen export from lowland artificial watersheds (polders). Water Res. 133, 319–337.

Huang, Q., Zhang, W., 2010. Application and parameters sensitivity analysis of SWAT model. Arid. Land Geogr. 33 (1), 8–15.

Javaheri, A., Babbar-Sebens, M., Alexander, J., Bartholomew, J., Hallett, S., 2018. Global sensitivity analysis of water age and temperature for informing salmonid disease management. J. Hydrol. 561, 89–97.

Jia, Y., 2016. Spatio-temporal Patterns of Atmospheric Nitrogen Depositon in China and Global Land. University of Chinese Academy of Sciences, Beijing.

Jin, S., Zhou, J., Bao, W., Chen, J., Li, D., Li, Y., 2017. Comparison of nitrogen and phosphorus uptake and water purification ability of five submerged macrophytes. Environ. Sci. 38 (1), 156–161.

Krause, P., Boyle, D., Bäse, F., 2005. Comparison of Different Efficiency Criteria for Hydrological Model Assessment.

Lai, G., Yu, G., Gui, F., 2006. Preliminary study on assessment of nutrient transport in the Taihu Basin based on SWAT modeling. Sci. China, Ser. A D 49 (1), 135–145.

Lai, Z., Li, S., Deng, Y., Lv, G., Ullah, S., 2018. Development of a polder module in the SWAT model: SWATpld for simulating polder areas in south-eastern China. Hydrol. Process. 32 (8), 1050–1062.

Legates, D.R., McCabe Jr., G.J., 1999. Evaluating the use of "goodness-of-fit" measures in hydrologic and hydroclimatic model validation. Water Resour. Res. 35 (1), 233–241.

Li, S., Lai, Z., Wang, Q., Wang, Z., Li, C., Song, X., 2013. Distributed simulation for hydrological process in plain river network region using SWAT model. Trans. Chin. Soc. Agric. Eng. 29 (6), 106–112.

Li, Z., Luo, C., Xi, Q., Li, H., Pan, J., Zhou, Q., Xiong, Z., 2015. Assessment of the AnnAGNPS model in simulating runoff and nutrients in a typical small watershed in the Taihu Lake basin, China. Catena 133, 349–361.

Lian, H., Lei, Q., Zhang, X., Yen, H., Wang, H., Zhai, L., Liu, H., Huang, J.-C., Tianzhi, R., Jiaogen, Z., Weiwen, Q., 2018. Effects of anthropogenic activities on long-term changes of nitrogen budget in a plain river network region: a case study in the Taihu Basin. Sci. Total Environ. 645, 1212–1220.

Liang, H., Yang, S.H., Xu, J.Z., Hu, K.L., 2021. Modeling water consumption, N fates, and rice yield for water-saving and conventional rice production systems. Soil Tillage Res. 209, 10.

Lukianas, A., Vaikasas, S., Malisauskas, A.P., 2006. Water management tasks in the summer polders of the Nemunas Lowland. Irrigat. Drain.: The journal of the International Commission on Irrigation and Drainage 55 (2), 145–156.

Luo, Y., Su, B., Yuan, J., Li, H., Zhang, Q., 2011. GIS techniques for watershed delineation of SWAT model in plain polders. Procedia Environmental Sciences 10, 2050–2057.

Malhi, S.S., Lemke, R., Wang, Z., Chhabra, B.S., 2006. Tillage, nitrogen and crop residue effects on crop yield, nutrient uptake, soil quality, and greenhouse gas emissions. Soil Tillage Res. 90 (1–2), 171–183.

McCuen Richard, H., Knight, Z., Cutter, A.G., 2006. Evaluation of the nash–sutcliffe efficiency index. J. Hydrol. Eng. 11 (6), 597–602.

Menzel, R., 1980. Enrichment Ratios for Water Quality Modeling. CREAMS: A Field-Scale Model for Chemicals, Runoff, and Erosion from Agricultural Management Systems Conservation Research Report Number 26, May, pp. 486–492, 1980, 1 Fig, 2 Tab, 11 Ref.

Miao, Y., Stewart, B.A., Zhang, F., 2011. Long-term experiments for sustainable nutrient management in China. A review. Agron. Sustain. Dev. 31 (2), 397–414.

Morris, M.D., 1991. Factorial sampling plans for preliminary computational experiments. Technometrics 33 (2), 161–174.

Neitsch, S., Arnold, J., Kiniry, J., Williams, J., 2011. Soil & Water Assessment Tool—Theoretical Documentation Version 2009. Texas Water Resour. Inst.

Peng, S., Buresh, R.J., Huang, J., Zhong, X., Zou, Y., Yang, J., Wang, G., Liu, Y., Hu, R., Tang, Q., Cui, K., Zhang, F., Dobermann, A., 2010. Improving nitrogen fertilization in rice by sitespecific N management. A review. Agron. Sustain. Dev. 30 (3), 649–656.

Reynolds Puga, J.E., Halldin, S., Seibert, J., Xu, C.-y., 2018. Effects on Rainfall-Runoff Models from Different Definitions of the Climatological and Discharge Day, p. 15601.

Sadeghi, S., Gholami, L., Khaledi Darvishan, A., Saeidi, P., 2014. A review of the application of the MUSLE model worldwide. Hydrol. Sci. J. 59 (2), 365–375.

Satman, M., 2013. Machine coded genetic algorithms for real parameter optimization problems. Gazi University Journal of Science 26 (1), 85–95.

Shi, K., Zhang, Y., Zhu, G., Liu, X., Zhou, Y., Xu, H., Qin, B., Liu, G., Li, Y., 2015. Long-term remote monitoring of total suspended matter concentration in Lake Taihu using 250m MODIS-Aqua data. Rem. Sens. Environ. 164, 43–56.

Smith, R., Williams, J., 1980. Simulation of the surface water hydrology. Conserv. Res. Rep. (26), 13–35.

Su, B., Luo, Y., 2019. Modelling hydrological processes and nutrient retention in plain polders. Hydrol. Sci. J. 64 (7), 835–844.

Sun, B., 2013. Simulation of Agricultural Nonpoint Sources Pollution in the Monitoring Spots of Chaohu Lake on SWAT Model. Anhui Agricultural University, Hefei.

Taihu-Basin-Authority-of-Ministry-Of-Water-Resources, 2013. External Nutrient Loading of Lake Taihu in 2013. Shanghai.

Wade, A., Whitehead, P., Butterfield, D., 2002a. The Integrated Catchments model of Phosphorus dynamics (INCA-P), a new approach for multiple source assessment in heterogeneous river systems: model structure and equations. Hydrol. Earth Syst. Sci. Discuss. 6 (3), 583–606.

Wade, A.J., Durand, P., Beaujouan, V., Wessel, W.W., Raat, K.J., Whitehead, P.G., Butterfield, D., Rankinen, K., Lepisto, A., 2002b. A nitrogen model for European catchments: INCA, new model structure and equations. Hydrol. Earth Syst. Sci. Discuss. 6 (3), 559–582.

Wang, F., Shang, X., Bai, J., 2007. The Comprehensive Treatment Technology and Practice of Water Environment in Polder Areas of Plain Water Network. Southeast University Press, Nanjing.

Wang, P., 2006. Study and Application of Non-point Source Pollution Model of River Network Area Based on Digital Basin System. Hohai University, Nanjing.

Wang, Q., 1991. The genetic algorithm and its application to calibrating conceptual rainfall-runoff models. Water Resour. Res. 27 (9), 2467–2471.

Wang, T., Tang, L., Liu, J., 2011. Simulation and analysis of non-point source pollution in the polder region of Dongting Lake. Shui Li Fa Dian Xue Bao 30 (5), 27–34.

Wang, W.-H., Wang, Y., Li, Z., Wei, C.-Z., Zhao, J.-C., Sun, L.-q., 2018. Effect of a strengthened ecological floating bed on the purification of urban landscape water supplied with reclaimed water. Sci. Total Environ. 622–623, 1630–1639.

Wang, Y., Tabari, H., Xu, Y., Willems, P., 2010. Atmospheric and human-induced impacts on temporal variability of water level extremes in the Taihu Basin, China. Journal of Flood Risk Management 29 (8), 1571–1575.

Wang, Y., Tabari, H., Xu, Y., Willems, P., 2019. Atmospheric and human-induced impacts on temporal variability of water level extremes in the Taihu Basin, China. Journal of Flood Risk Management, e12539.

Wellen, C., Kamran-Disfani, A.-R., Arhonditsis, G.B., 2015. Evaluation of the current state of distributed watershed nutrient water quality modeling. Environ. Sci. Technol. 49 (6), 3278–3290.

Whitehead, P.G., Wilson, E.J., Butterfield, D., 1998. A semi-distributed Integrated Nitrogen model for multiple source assessment in Catchments (INCA): Part I — model structure and process equations. Sci. Total Environ. 210–211, 547–558.

Williams, J.R., Berndt, H.D., 1977. Sediment yield prediction based on watershed hydrology. Transactions of the ASAE 20 (6), 1100–1104.

Williams, J.R., Singh, V.P., 1995. The EPIC model.

Xu, A., 2007. Principle and Model Study of Agricultural Nonpoint Source Pollution of Representative Polder Area in Taihu Lake Basin. Hohai University, Nanjing.
Yan, R., Gao, J., Dong, C., Huang, J., 2015. Assessment of ecosystem services for polder terrestrial ecosystem in Taihu Basin. Research of Environmental Sciences 28 (3), 393–400.
Yan, R., Gao, J., Huang, J., 2019. Modelling the hydrological processes of a Chinese lowland polder and identifying the key factors using an improved PHPS model. J. Hydrol 578, 124083.
Yan, R., Huang, J., Li, L., Gao, J., 2017. Hydrology and phosphorus transport simulation in a lowland polder by a coupled modeling system. Environ. Pollut. 227, 613–625.
Yan, R., Li, L., Gao, J., 2018. Modelling the regulation effects of lowland polder with pumping station on hydrological processes and phosphorus loads. Sci. Total Environ. 637, 200–207.
Yan, R.H., Gao, J.F., Huang, J.C., 2016. WALRUS-paddy model for simulating the hydrological processes of lowland polders with paddy fields and pumping stations. Agric. Water Manag. 169, 148–161.
Yang, S., He, H., Lu, S., Chen, D., Zhu, J., 2008. Quantification of crop residue burning in the field and its influence on ambient air quality in Suqian, China. Atmos. Environ. 42 (9), 1961–1969.
Young, R.A., Onstad, C.A., Bosch, D.D., Anderson, W.P., 1989. AGNPS: a non-point-source pollution model for evaluating agricultural watersheds. J. Soil Water Conserv. 44 (2), 168–173.
Yu, C., Huang, X., Chen, H., Godfray, H.C.J., Wright, J.S., Hall, J.W., Gong, P., Ni, S., Qiao, S., Huang, G., Xiao, Y., Zhang, J., Feng, Z., Ju, X., Ciais, P., Stenseth, N.C., Hessen, D.O., Sun, Z., Yu, L., Cai, W., Fu, H., Huang, X., Zhang, C., Liu, H., Taylor, J., 2019. Managing nitrogen to restore water quality in China. Nature 567 (7749), 516–520.
Zhang, Y., Shi, K., Liu, X., Zhou, Y., Qin, B., 2014. Lake Topography and Wind Waves Determining Seasonal-Spatial Dynamics of Total Suspended Matter in Turbid Lake Taihu, China: Assessment Using Long-Term High-Resolution MERIS Data, e98055.
Zhao, G.J., Hörmann, G., Fohrer, N., Gao, J., Li, H., Tian, P., 2010. Application of a simple raster-based hydrological model for streamflow prediction in a humid catchment with polder systems. Water Resour. Manag. 25 (2), 661–676.
Zhao, G.J., Hörmann, G., Fohrer, N., Li, H.P., Gao, J.F., Tian, K., 2011. Development and application of a nitrogen simulation model in a data scarce catchment in South China. Agric. Water Manag. 98 (4), 619–631.
Zhao, R.J., 1992. The Xinanjiang model applied in China. J. Hydrol 135 (1), 371–381.
Zhao, X., Zhou, Y., Wang, S., Xing, G., Shi, W., Xu, R., Zhu, Z., 2012. Nitrogen balance in a highly fertilized rice–wheat double-cropping system in southern China. Soil Sci. Soc. Am. J. 76 (3), 1068–1078.
Zhou, Y., Si, Y., Zhao, X., Qingqian, W., Xu, H., Wang, S., Xing, G., 2012. Situation, problems and countermeasures in nitrogen fertilization in rice-wheat rotation paddy field of Taihu Lake Watershed, China. Soils 44 (3), 510–514.
Zhu, J., Xu, X., He, S., 2014. An analysis of parameter sensitivity of SWMM model based on LH-OAT method. China Rural Water and Hydropower (3), 84–87.
Zhu, Q., 2010. Research on Non-point Source Pollution Law and Regulated Simulation in Typical Areas of Plain River Netword Region. Nanjing hydraulic research institute, Nanjing.